DENSITY CUMULANT THEORY

FOR GROUND AND EXCITED ELECTRONIC STATES

by

ANDREAS VICTOR COPAN

(Under the Direction of Henry F. Schaefer III)

ABSTRACT

Here is my abstract.

INDEX WORDS: Electronic structure theory

DENSITY CUMULANT THEORY

FOR GROUND AND EXCITED ELECTRONIC STATES

by

ANDREAS VICTOR COPAN

B.A., Bethel University, 2013

A Dissertation Submitted to the Graduate Faculty

of The University of Georgia in Partial Fulfillment

of the

Requirements for the Degree

DOCTOR OF PHILOSOPHY

ATHENS, GEORGIA

2018

Density Cumulant Theory

for Ground and Excited Electronic states

by

Andreas Victor Copan

Approved:

Major Professor: Henry F. Schaefer III

Committee: Gary E. Douberly
                    Henning Meyer

Electronic Version Approved:

Suzanne Barbour
Dean of the Graduate School
The University of Georgia
December 2018

In memory of Valery Andreiyevich and Valtraut Kirsch Copan

Acknowledgments

All of your acknowledgments should go here.

Contents

Chapter 1

Introduction

Here is the introduction.

Chapter 2

Ground-State Density Cumulant Theory: Thermochemical and Kinetic Benchmark Calculations[*]

2.1 Abstract

We present an extensive benchmark study of density cumulant functional theory (DCFT) for thermochemistry and kinetics of closed- and open-shell molecules. The performance of DCFT methods (DC-06, DC-12, ODC-06, and ODC-12) is compared to that of coupled-electron pair methods ($CEPA_0$ and $OCEPA_0$) and coupled-cluster theory (CCSD and CCSD(T)) for the description of noncovalent interactions (A24 database), barrier heights of hydrogen-transfer reactions (HTBH38), radical stabilization energies (RSE30), adiabatic ionization energies (AIE), and covalent bond stretching in diatomic molecules. Our results indicate that out of four DCFT methods the ODC-12 method is the most reliable and accurate DCFT formulation to date. Compared to CCSD, ODC-12 shows superior results for all benchmark tests employed in our study. With respect to coupled-pair

---

theories, ODC-12 outperforms $CEPA_0$, and shows similar accuracy to the orbital-optimized $CEPA_0$ variant ($OCEPA_0$) for systems at equilibrium geometries. For covalent bond stretching, ODC-12 is found to be more reliable than $OCEPA_0$. For the RSE30 and AIE datasets, ODC-12 shows competitive performance with CCSD(T). In addition to benchmark results, we report new reference values for the RSE30 dataset computed using coupled cluster theory with up to perturbative quadruple excitations.

2.2 Introduction

Recent developments in *ab initio* quantum chemistry have resulted in a variety of computational models for studying molecules. Apart from concerns about efficiency and accuracy, several concepts have evolved as criteria for judging the merits of a particular method. Energy-based criteria typically define an "ideal" approximation as one yielding correlation energies that are size-consistent, extensive[1], well-defined (giving continuous, unique potential surfaces), and variational.[2] While it has been argued that the practical benefits of variationality are rather limited,[3] the efficiency of gradient computations, at least, is improved by formulating a theory in terms of a Hermitian and stationary energy functional.[4] With respect to scope and stability, methods that show consistent performance for open-shell systems, strongly correlated states, and non-equilibrium geometries are particularly valuable.[3]

The incorrect scaling of truncated configuration interaction (CI) energies with system size has inspired the development of size-extensive alternatives. Among

3

the earliest formulations, the coupled electron pair approximations (CEPAs)[5–9] attracted much attention in 1970s,[10–14] offering rigorous extensivity and size-consistency while retaining much of the linearity[15] of CI in their equations. CEPA methods, however, have been shown to rapidly deteriorate as the molecular geometry deviates from equilibrium[15] and yield energies that vary under the rotation of the occupied orbitals.[8] Partly in light of such defects, CEPA has been largely displaced by coupled-cluster (CC) theory.[3;16–22] In addition to size-extensivity, CC offers orbital invariance and improved stability for non-equilibrium structures[15], but has a non-Hermitian energy functional and non-linear equations which are not readily amenable to parallel implementation. Although neither class of methods is strictly variational, VCEPA (variational CEPA) has been shown to be effectively equivalent to its non-variational counterpart.[23] Various other modifications to resolve the deficiencies of traditional CEPA have been explored, including self-consistent size-consistent CI,[24;25] orbital-invariant CEPA,[26;27] and orbital-optimized CEPA formulations.[28–31] Recently, the CEPA methods have been revived by Neese and co-workers[23;32;33] who developed the local pair-natural-orbital CEPA (LPNO-CEPA) methods and have implemented them for massively parallel computer architectures.

It has recently been demonstrated[34–37] that CEPA methods naturally arise in the context of theories that obtain the molecular energies from density cumulants, the connected and extensive components of the reduced density matrices (RDMs).[38–43] The advantage of cumulant-based theories is that, unlike their RDM-based counterparts,[44–46] they are naturally size-extensive and size-consistent.[41;47]

4

We have recently achieved the first implementation[48;49] of density cumulant functional theory (DCFT), proposed by Kutzelnigg in 2006.[34] In DCFT, the molecular energy is obtained in terms of a mean-field one-particle RDM and the two-particle density cumulant, constrained to be at least approximately N-representable (*i.e.* to correspond to a physical N-electron wavefunction). Like traditional CC theory, DCFT is size-extensive and orbital-invariant, but it has the additional advantage of a stationary and Hermitian energy functional, which simplifies the computation of molecular properties. In the original DCFT formulation (DC-06)[34;48;49] N-representability conditions derived from second-order Møller-Plesset perturbation theory (MPPT) were used,[50] yielding equations similar to those of the simplest CEPA model (CEPA$_0$),[7;9] but including higher-order terms in the description of one-particle correlation effects. Using the same set of conditions, we have developed new formulations of DCFT that take advantage of an improved description of the one-particle density matrix (DC-12)[51] and full orbital optimization (ODC-06 and ODC-12 methods).[52]

Our previous studies[48;49;51;52] demonstrated for a limited set of systems that the DC-06, DC-12, ODC-06 and ODC-12 methods generally yield molecular energies and properties competitive with those obtained by CCSD and CCSD(T), but may exhibit unstable performance due to imbalances in the description of electron correlation. Herein, we present an extensive benchmark of the DCFT methods with respect to thermochemical and kinetic molecular properties, including noncovalent interactions, barrier heights in hydrogen-transfer reactions, radical stabilization energies, and adiabatic ionization energies for challenging electron-

dense systems. We conclude our benchmark study by testing the performance of DCFT for covalent bond stretching in diatomic molecules.

2.3 Overview of DCFT

In this section a short overview of DCFT is presented. For details on the theory the reader is referred to our earlier publications.[48;51;52] In the RDM methods[53] the exact molecular energy is expressed as a functional of the one- and two-particle reduced density matrices, $\boldsymbol{\gamma}_1$ and $\boldsymbol{\gamma}_2$ (1-RDM and 2-RDM):

$$E = h_p^q \gamma_q^p + \tfrac{1}{2} g_{pq}^{rs} \gamma_{rs}^{pq} \ , \qquad [\boldsymbol{\gamma}_1]_q^p \equiv \gamma_q^p \ , \qquad [\boldsymbol{\gamma}_2]_{rs}^{pq} \equiv \gamma_{rs}^{pq} \ . \qquad (2.1)$$

In eq. (2.1), h_p^q and g_{pq}^{rs} are the usual one- and two-electron integrals in the orthonormal spin-orbital basis $\{\psi_p\}$ and summation over the repeated indices is implied. Expressing $\boldsymbol{\gamma}_1$ through $\boldsymbol{\gamma}_2$ via the partial trace relation $\sum_r \gamma_{qr}^{pr} = (N-1)\gamma_q^p$, the energy functional (2.1) can be minimized by varying $\boldsymbol{\gamma}_2$ subject to N-representability constraints. This is the essence of the variational 2-RDM approach.[53]

In DCFT, some of the challenges of the 2-RDM approach are circumvented by expanding $\boldsymbol{\gamma}_2$ in terms of its irreducible components – the 1-RDM and the two-particle cumulant (denoted by $\boldsymbol{\lambda}_2$):

$$\gamma_{rs}^{pq} = \gamma_r^p \gamma_s^q - \gamma_r^q \gamma_s^p + \lambda_{rs}^{pq} \ . \qquad (2.2)$$

In eq. (2.2), $\boldsymbol{\lambda}_2$ describes the correlated part of $\boldsymbol{\gamma}_2$ that cannot be expressed via $\boldsymbol{\gamma}_1$. The cumulant also determines the correlation contribution to $\boldsymbol{\gamma}_1$, allowing

the 1-RDM to be decomposed as the sum of an idempotent 1-RDM ($\boldsymbol{\kappa}$) and a correlation correction ($\boldsymbol{\tau}$):

$$\boldsymbol{\gamma}_1 = \boldsymbol{\kappa} + \boldsymbol{\tau}. \tag{2.3}$$

The correlation component $\boldsymbol{\tau}$ is fully specified by $\boldsymbol{\lambda}_2$, whereas $\boldsymbol{\kappa}$ is independent of $\boldsymbol{\lambda}_2$. Equations (2.2) and (2.3) allow us to write an equivalent energy expression with $\boldsymbol{\kappa}$ and $\boldsymbol{\lambda}_2$ as independent functional parameters:

$$
\begin{aligned}
E[\boldsymbol{\kappa}, \boldsymbol{\lambda}_2] &= \tfrac{1}{2}(h_p^q + f_p^q)(\kappa_q^p + \tau_q^p) + \tfrac{1}{4}\overline{g}_{pq}^{rs}\lambda_{pq}^{rs}, \\
f_p^q &= h_p^q + \overline{g}_{pr}^{qs}(\kappa_s^r + \tau_s^r), \quad \overline{g}_{rs}^{pq} = g_{rs}^{pq} - g_{rs}^{qp}.
\end{aligned}
\tag{2.4}
$$

Here, the generalized Fock operator $\boldsymbol{f}$ differs from that of Hartree-Fock theory by the presence of an external potential $\overline{g}_{pr}^{qs}\tau_s^r$ due to electron correlation.[34]

To date, all DCFT formulations make the energy (2.4) stationary with respect to variations of $\boldsymbol{\lambda}_2$, subject to cumulant N-representability constraints derived from second-order Møller-Plesset perturbation theory (MPPT).[50] To account for orbital relaxation effects, the two earliest DCFT methods, DC-06[34;48;49] and DC-12[51], determined the orbitals by diagonalizing the generalized Fock operator $\boldsymbol{f}$ defined in eq. (2.4). These two methods differ in their description of 1-RDM N-representability. Whereas DC-06 employs an approximate expression for $\boldsymbol{\tau}$ in terms of $\boldsymbol{\lambda}_2$, DC-12 uses the exact relationship. Recently, we proposed orbital-optimized variants of DC-06 and DC-12 (ODC-06 and ODC-12),[52] which fully account for orbital relaxation effects.

2.4 Computational Details

All computations were performed using the Psi4 package.[54] The results were benchmarked against coupled cluster theory with single and double excitations (CCSD)[20–22], CCSD with perturbative triple excitations [CCSD(T)],[55;56] coupled electron pair approximation zero (CEPA$_0$),[7;9] and the orbital-optimized variant of CEPA$_0$ (OCEPA$_0$)[29]. All electrons were correlated in all computations. The cc-pCVXZ[57;58] and aug-cc-pVXZ[59] basis sets (X = T, Q) were used (see text for details). Noncovalent interaction energies, hydrogen-transfer barrier heights, and radical stabilization energies were computed using geometries from the A24[60], HTBH38[61], and RSE30[62] benchmark databases, respectively, available in Psi4. Adiabatic ionization energies were computed from neutral and cation geometries optimized at each level of theory, with added harmonic zero-point vibrational energy corrections. Harmonic frequencies were computed by numerical differentiation of analytic energy gradients. Single-point energies were converged to 10^{-8} E_{h}, while the root mean square of the energy gradient was converged to 10^{-6} E_{h}/a_0 for geometry optimizations.

2.5 Results and Discussion

2.5.1 Noncovalent Interactions

We begin by testing the accuracy of DCFT methods for the description of noncovalent interactions in 24 closed-shell molecular dimers, which are listed in table 2.1. These molecular complexes comprise the A24 dataset[60] developed by Řezáč and

8

Table 2.1: Errors in interaction energies (kcal mol^{-1}) for 24 noncovalently bound molecular dimers comprising the A24 database[60] computed using seven methods with the aug-cc-pVTZ basis set. The errors are relative to CCSD(T) reference values (kcal mol^{-1}) shown in the rightmost column. For each method the mean absolute deviations from CCSD(T) (Δ_{MAE}, kcal mol^{-1}) and the standard deviations from the mean signed error (Δ_{SD}, kcal mol^{-1}) are also shown.

Complex (Sym.)	ΔCEPA$_0$	ΔDC-06	ΔDC-12	ΔCCSD	ΔOCEPA$_0$	ΔODC-06	ΔODC-12	CCSD(T)
H$_2$O···NH$_3$ (C$_\text{s}$)	0.26	0.24	0.22	0.36	0.19	0.20	0.18	-7.18
H$_2$O···H$_2$O (C$_\text{s}$)	0.19	0.18	0.16	0.25	0.13	0.14	0.12	-5.71
HCN···HCN (C$_\text{s}$)	0.21	0.27	0.16	0.15	0.18	0.26	0.14	-7.12
HF···HF (C$_\text{s}$)	0.14	0.13	0.11	0.16	0.08	0.09	0.07	-5.20
NH$_3$···NH$_3$ (C$_\text{2h}$)	0.15	0.13	0.14	0.26	0.12	0.12	0.12	-3.43
HF···CH$_4$ (C$_\text{3v}$)	0.17	0.16	0.20	0.23	0.12	0.12	0.16	-2.30
NH$_3$···CH$_4$ (C$_\text{3v}$)	0.07	0.05	0.05	0.13	0.05	0.05	0.04	-1.08
H$_2$O···CH$_4$ (C$_\text{s}$)	0.06	0.05	0.04	0.11	0.05	0.05	0.04	-1.03
CH$_2$O···CH$_2$O (C$_\text{s}$)	0.89	0.99	0.65	0.46	0.62	0.87	0.46	-5.23
H$_2$O···C$_2$H$_4$ (C$_\text{s}$)	0.15	0.16	0.15	0.31	0.20	0.26	0.21	-3.33
CH$_2$O···C$_2$H$_4$ (C$_\text{s}$)	0.21	0.18	0.14	0.27	0.19	0.24	0.16	-2.24
HCCH···HCCH (C$_\text{2v}$)	0.07	0.05	0.05	0.20	0.10	0.12	0.10	-2.57

Complex (Sym.)	ΔCEPA$_0$	ΔDC-06	ΔDC-12	ΔCCSD	ΔOCEPA$_0$	ΔODC-06	ΔODC-12	CCSD(T)
NH$_3$···C$_2$H$_4$ (C$_s$)	0.09	0.06	0.08	0.24	0.12	0.15	0.13	-2.07
C$_2$H$_4$···C$_2$H$_4$ (C$_{2v}$)	0.10	0.02	0.07	0.33	0.14	0.13	0.15	-1.81
CH$_4$···C$_2$H$_4$ (C$_s$)	0.02	-0.02	0.01	0.14	0.05	0.04	0.06	-0.92
BH$_3$···CH$_4$ (C$_s$)	0.23	0.18	0.24	0.37	0.18	0.16	0.22	-2.52
CH$_4$···C$_2$H$_4$ (C$_s$)	0.13	0.09	0.13	0.23	0.10	0.09	0.09	-1.37
CH$_4$···C$_2$H$_6$ (C$_s$)	0.09	0.06	0.09	0.17	0.07	0.06	0.09	-1.14
CH$_4$···CH$_4$ (D$_{3d}$)	0.08	0.06	0.08	0.14	0.06	0.05	0.08	-0.93
Ar···CH$_4$ (C$_{3v}$)	0.07	0.05	0.07	0.10	0.05	0.05	0.06	-0.78
Ar···C$_2$H$_4$ (C$_{2v}$)	0.03	-0.01	0.02	0.11	0.05	0.03	0.05	-0.63
C$_2$H$_4$···HCCH (C$_{2v}$)	-0.02	-0.19	-0.01	0.38	0.07	-0.06	0.11	0.43
C$_2$H$_4$···C$_2$H$_4$ (D$_{2h}$)	-0.05	-0.30	-0.03	0.43	0.04	-0.16	0.11	0.41
HCCH···HCCH (D$_{2h}$)	0.01	-0.09	0.02	0.34	0.10	0.02	0.12	0.91
Δ_{MAE}:	0.14	0.16	0.12	0.25	0.13	0.15	0.13	
Δ_{SD}:	0.18	0.23	0.13	0.11	0.12	0.18	0.09	

Hobza to include a variety of noncovalent interactions, including hydrogen bonding and π-π stacking. Although Řezáč and Hobza reported the interaction energies at the CCSD(T) complete basis set (CBS) limit, we use CCSD(T)/aug-cc-pVTZ energies as reference values in order to effectively exclude basis-set incompleteness error from the comparison.

Figure 2.1 depicts mean absolute error (Δ_{MAE}) relative to CCSD(T) in the binding energies of CEPA$_0$, OCEPA$_0$, CCSD, and the four DCFT methods (DC-06, DC-12, ODC-06, and ODC-12), as well as the root mean square deviation from the average signed error (Δ_{SD}). All methods but CCSD give similar Δ_{MAE} values (0.14 ± 0.02 kcal mol^{-1}), and a comparison between CEPA$_0$, DC-06, and DC-12 and their orbital-optimized variants (OCEPA$_0$, ODC-06, and ODC-12) shows negligible 0.01 kcal mol^{-1} differences in each case. CCSD gives a significantly larger Δ_{MAE} (0.25 kcal mol^{-1}) than the other methods, exceeding the DC-12 Δ_{MAE} by a factor of two (0.12 kcal mol^{-1}). The Δ_{SD} values are much more sensitive to the choice of method than the Δ_{MAE} values, and are noticeably affected by orbital optimization. ODC-12 gives the smallest standard deviation ($\Delta_{\mathrm{SD}} = 0.09$ kcal mol^{-1}), while the largest Δ_{SD} value was found for DC-06 (0.23 kcal mol^{-1}). The OCEPA$_0$, ODC-06, and ODC-12 methods ($\Delta_{\mathrm{SD}} = 0.12$, 0.18, and 0.09 kcal mol^{-1}, respectively) exhibit much more consistent performance than their non-orbital-optimized analogues, with Δ_{SD} smaller by 0.05 ± 0.01 kcal mol^{-1} in each case. CCSD also exhibits a relatively small Δ_{SD} value (0.11 kcal mol^{-1}), possibly due to its inclusion of single excitations which partly account for orbital relaxation.

Errors in interaction energy and CCSD(T) reference values for each molecular
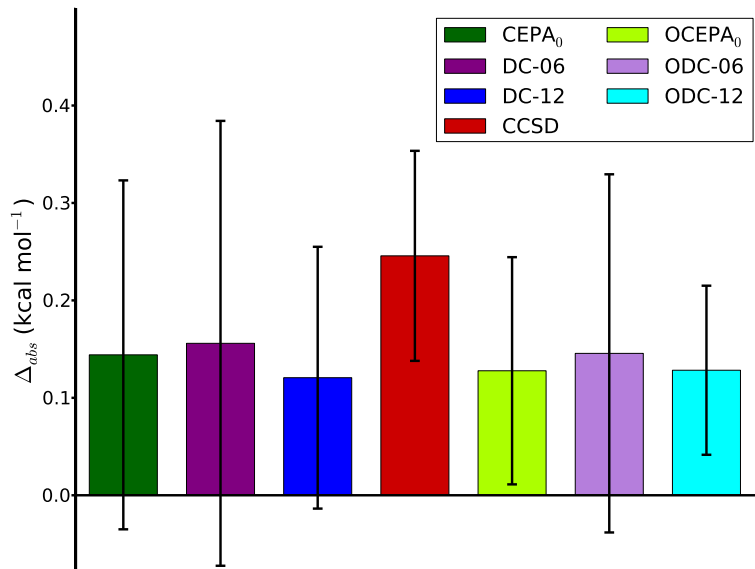
Figure 2.1: Mean absolute deviations (Δ_{MAE}, kcal mol^{-1}) and the standard deviations from the mean signed error (Δ_{SD}, kcal mol^{-1}) of the interaction energies for 24 noncovalently bound molecular dimers (A24 database) computed using seven methods with the aug-cc-pVTZ basis set. The errors are relative to CCSD(T)/aug-cc-pVTZ reference values. The Δ_{MAE} value is represented as a height of each colored box, while the Δ_{SD} value is depicted as a radius of the black vertical bar. See table 2.1 for data on individual database members.

complex are shown in table 2.1. The largest deviations from CCSD(T) were obtained for the formaldehyde dimer ($CH_2O \cdots CH_2O$, complex 9 in table 2.1), for which DC-06, CEPA$_0$, and OCEPA$_0$ yield errors of 0.99, 0.89, and 0.87 kcal mol^{-1}, respectively. For this system, the best performance is shown by CCSD and ODC-12, both of which give an error of 0.46 kcal mol^{-1}. For systems with π-stacking

interactions (complexes 22-24 in table 2.1), CCSD shows large errors (0.38, 0.43, 0.34 kcal mol^{-1}) relative to the magnitude of the interaction energy (0.43, 0.41, 0.91 kcal mol^{-1}, respectively). Here CEPA$_0$, DC-12, and their orbital-optimized variants offer much better agreement with CCSD(T), with errors ranging from 0.01 to 0.15 kcal mol^{-1}.

2.5.2 Hydrogen-Transfer Reaction Barrier Heights

We continue by assessing the performance of DCFT methods in predicting barrier heights for 18 hydrogen-transfer reactions from the HTBH38 database:[61]

$$R_1 + R_2H \longrightarrow [R_1R_2H]^* \longrightarrow R_1H + R_2 \qquad (2.5)$$
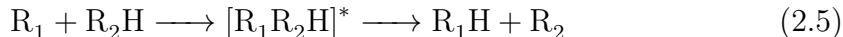
These reactions† involve molecules (R$_1$ and R$_2$) and transition states ($[R_1R_2H]^*$) with open-shell character, making their properties more sensitive to electron correlation effects. We employ barrier heights computed at the CCSD(T)/aug-cc-pVTZ level of theory as our reference rather than the values provided by Lynch[63] in order to effectively exclude basis-set incompleteness effects. We also omit the DC-06 and ODC-06 methods, which encounter frequent convergence problems due to the poor description of N-representability (see Supporting Information for incomplete DC-06 results).

Mean absolute deviations (Δ_{MAE}) and standard deviations (Δ_{SD}) for the hydrogen-transfer barrier heights are presented in table 2.2 and plotted in fig. 2.2. The

---

†Reaction 19 in HTBH38, the cis-trans isomerization of piperylene, is omitted in the present study.

Table 2.2: Errors in barrier heights (kcal mol^{-1}) for 18 hydrogen-transfer reactions ($R_1 + R_2H \rightarrow R_1H + R_2$) comprising the HTBH38 database[63] computed using five methods with the aug-cc-pVTZ basis set. The errors are relative to CCSD(T) reference values (kcal mol^{-1}) shown in the rightmost column. Each reaction includes barrier heights in the forward ($R_1 + R_2H \rightarrow [R_1R_2H]^*$) and reverse ($[R_1R_2H]^* \leftarrow R_1H + R_2$) directions, respectively, except in the case of $R_1 = R_2 = H$ where they are the same. The mean absolute (Δ_{MAE}, kcal mol^{-1}) and the mean percent (Δ_{rel}, %) errors with respect to CCSD(T), as well as the standard deviations from the mean signed error (Δ_{SD}, kcal mol^{-1}) are also shown.

	Reaction Barrier	ΔCEPA$_0$	ΔDC-12	ΔCCSD	ΔOCEPA$_0$	ΔODC-12	CCSD(T)
1	H + HCl$\rightarrow$[HHCl]*	0.74	0.49	0.09	-0.41	-0.28	5.22
2	OH + H$_2$$\rightarrow$[OHH$_2$]*	3.77	3.38	1.82	0.88	1.24	4.99
3	CH$_3$ + H$_2$$\rightarrow$[CH$_3H_2$]*	1.60	1.46	1.37	0.46	0.70	11.29
4	OH + CH$_4$$\rightarrow$[OHCH$_4$]*	4.26	3.85	2.61	1.22	1.65	5.64
5	H + H$_2$$\rightarrow$[HH$_2$]*	0.80	0.69	0.30	-0.27	-0.05	9.77
6	OH + NH$_3$$\rightarrow$[OHNH$_3$]*	6.02	5.25	3.54	1.18	1.82	3.17
7	HCl + CH$_3$$\rightarrow$[HClCH$_3$]*	1.93	1.78	1.79	0.68	0.92	0.10
8	OH + C$_2$H$_6$$\rightarrow$[OHC$_2H_6$]*	4.66	4.21	2.69	1.28	1.72	2.69
9	F + H$_2$$\rightarrow$[FH$_2$]*	3.40	3.14	1.20	0.52	0.78	1.13
10	O + CH$_4$$\rightarrow$[OHCH$_3$]*	3.40	3.12	2.37	0.70	1.20	13.62
11	H + PH$_3$$\rightarrow$[HPH$_3$]*	0.93	0.86	0.59	-0.16	0.10	2.29
12	H + HO$\rightarrow$[OHH]*	2.03	1.59	0.44	-0.61	-0.26	10.25
13	H + H$_2$S$\rightarrow$[HH$_2$S]*	1.01	0.92	0.65	-0.11	0.14	3.17
14	O + HCl$\rightarrow$[OHCl]*	6.33	6.01	3.58	0.79	1.51	9.74
15	NH$_2$ + CH$_3$$\rightarrow$[CH$_3NH_2$]*	2.48	2.22	1.99	0.49	0.86	7.66
16	NH$_2$ + C$_2$H$_5$$\rightarrow$[NH$_2C_2H_5$]*	2.48	2.22	2.09	0.55	0.92	8.21
17	C$_2$H$_6$ + NH$_2$$\rightarrow$[C$_2H_6NH_2$]*	3.30	3.00	2.73	1.23	1.62	10.39
18	NH$_2$ + CH$_4$$\rightarrow$[NH$_2CH_4$]*	2.98	2.72	2.55	1.11	1.48	13.23

	Reaction Barrier	ΔCEPA_0	$\Delta\text{DC-12}$	ΔCCSD	ΔOCEPA_0	$\Delta\text{ODC-12}$	CCSD(T)
1	$[\text{HHCl}]^*\leftarrow\text{H}_2 + \text{Cl}$	1.44	1.31	1.61	0.53	0.77	7.39
2	$[\text{OHH}_2]^*\leftarrow\text{H} + \text{H}_2\text{O}$	2.09	1.66	0.09	-0.91	-0.58	21.07
3	$[\text{CH}_3\text{H}_2]^*\leftarrow\text{H} + \text{CH}_4$	0.95	0.80	0.38	-0.38	-0.11	14.91
4	$[\text{OHCH}_4]^*\leftarrow\text{CH}_3 + \text{H}_2\text{O}$	3.23	2.80	1.87	0.27	0.65	18.09
6	$[\text{OHNH}_3]^*\leftarrow\text{H}_2\text{O} + \text{NH}_2$	5.46	4.62	3.14	0.79	1.33	13.17
7	$[\text{HClCH}_3]^*\leftarrow\text{Cl} + \text{CH}_4$	1.97	1.94	2.31	0.78	1.16	5.89
8	$[\text{OHC}_2\text{H}_6]^*\leftarrow\text{H}_2\text{O} + \text{C}_2\text{H}_5$	3.34	2.89	1.85	0.28	0.64	18.49
9	$[\text{FH}_2]^*\leftarrow\text{HF} + \text{H}$	1.27	0.88	-0.78	-1.47	-1.33	32.95
10	$[\text{OHCH}_3]^*\leftarrow\text{OH} + \text{CH}_3$	2.62	2.29	1.82	0.32	0.68	7.43
11	$[\text{HPH}_3]^*\leftarrow\text{PH}_2 + \text{H}_2$	1.14	1.11	1.37	0.39	0.63	23.21
12	$[\text{OHH}]^*\leftarrow\text{H}_2 + \text{O}$	3.47	3.08	1.99	0.62	1.07	12.81
13	$[\text{HH}_2\text{S}]^*\leftarrow\text{H}_2 + \text{HS}$	1.51	1.51	1.88	0.65	0.97	16.41
14	$[\text{OHCl}]^*\leftarrow\text{OH} + \text{Cl}$	5.59	5.35	3.55	0.51	1.24	9.35
15	$[\text{CH}_3\text{NH}_2]^*\leftarrow\text{CH}_4 + \text{NH}$	2.77	2.49	2.26	0.73	1.12	21.32
16	$[\text{NH}_2\text{C}_2\text{H}_5]^*\leftarrow\text{C}_2\text{H}_6 + \text{NH}$	3.06	2.75	2.46	0.85	1.26	18.52
17	$[\text{C}_2\text{H}_6\text{NH}_2]^*\leftarrow\text{NH}_3 + \text{C}_2\text{H}_5$	2.54	2.30	2.30	0.63	1.02	16.20
18	$[\text{NH}_2\text{CH}_4]^*\leftarrow\text{CH}_3 + \text{NH}_3$	2.51	2.29	2.21	0.56	0.96	15.69
	Δ_{MAE}:	2.77	2.49	1.84	0.67	0.94	
	Δ_{SD}:	1.51	1.39	1.06	0.62	0.71	
	Δ_{rel} %:	99	90	77	29	40	

largest Δ_{MAE} values come from CEPA_0 and DC-12 (2.77 and 2.49 kcal mol^{-1}, respectively). Orbital optimization greatly improves the accuracy of these methods, resulting in Δ_{MAE} values of just 0.67 and 0.94 kcal mol^{-1} for OCEPA_0 and ODC-12, respectively. The CCSD method shows intermediate performance with Δ_{MAE} = 1.84 kcal mol^{-1}. A similar trend is observed for the Δ_{SD} values, with OCEPA_0 (0.62 kcal mol^{-1}) and ODC-12 (0.71 kcal mol^{-1}) significantly improving upon CEPA_0 (1.51 kcal mol^{-1}), DC-12 (1.39 kcal mol^{-1}), and CCSD (1.06 kcal mol^{-1}). In addition to Δ_{MAE} and Δ_{SD}, table 2.2 includes mean percent error (Δ_{rel}) values, which are commonly used to benchmark performance for reaction kinetics. The smallest Δ_{rel} values are 29% and 40% for OCEPA_0 and ODC-12, respectively.

Turning to barrier heights for individual hydrogen-transfer reactions (table 2.2), the largest errors are observed for reactions 6 and 14, both involving the OH radical, for which CEPA_0 and DC-12 give errors of $\sim$ 5-6 kcal mol^{-1}. The best results for these reactions are obtained from OCEPA_0, with errors ranging from 0.51 to 1.18 kcal mol^{-1}. The ODC-12 method tends to predict larger barrier heights than OCEPA_0, yielding smaller errors only when OCEPA_0 underestimates the barrier heights.

2.5.3 Radical Stabilization Energies

In this section we study the performance of DCFT methods for predicting radical stabilization energies (RSEs). An R-group's RSE is defined as the enthalpy of a

Figure 2.2: Mean absolute deviations (Δ_{MAE}, kcal mol^{-1}) and the standard deviations from the mean signed error (Δ_{SD}, kcal mol^{-1}) of barrier heights for 18 hydrogen-transfer reactions ($R_1 + R_2H \rightarrow R_1H + R_2$, HTBH38 database) computed using five methods with the aug-cc-pVTZ basis set. The errors are relative to CCSD(T)/aug-cc-pVTZ reference values. The Δ_{MAE} value is represented as a height of each colored box, while the Δ_{SD} value is depicted as a radius of the black vertical bar. See table 2.2 for data on individual database members.
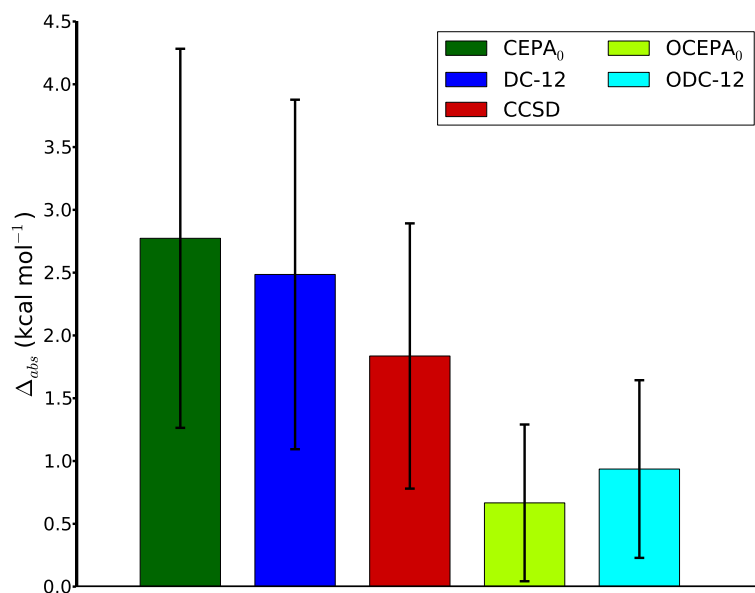
Table 2.3: Errors in radical stabilization energies (RSEs, kcal mol^{-1}) for 30 open-shell doublet species ($\cdot$R) comprising the RSE30 database[62] computed using six methods with the cc-pCVTZ basis set. The errors are relative to CCSD(T) with an added quadruples correction ($\delta Q = E_{\mathrm{CCSDT(Q)}} - E_{\mathrm{CCSD(T)}}$) shown in the rightmost column in kcal mol^{-1}. The δQ correction was computed using the cc-pCVDZ basis set. RSE is defined as the reaction enthalpy for the homodesmotic reaction $\cdot$CH$_3$ + RH → CH$_4$ + $\cdot$R. To indicate the degree of spin-contamination in the UHF reference, the spin expectation values ($\langle \hat{S}^2 \rangle_{\mathrm{SCF}}$) are also shown in units of $\hbar^2$. For each method the mean absolute deviations from CCSD(T)+δQ (Δ_{MAE}, kcal mol^{-1}) and the standard deviations from the mean signed error (Δ_{SD}, kcal mol^{-1}) are also presented.

$\cdot$R	$\langle \hat{S}^2 \rangle_{\mathrm{SCF}}$	ΔCEPA$_0$	ΔDC-12	ΔCCSD	ΔOCEPA$_0$	ΔODC-12	ΔCCSD(T)	CCSD(T)+δQ
$\cdot$CH$_2$NO$_2$	0.78	1.24	0.95	0.66	0.16	0.27	0.32	-3.50
$\cdot$CH$_2$OCHO	0.76	1.16	1.12	0.63	0.40	0.48	0.10	-4.84
$\cdot$CH$_2$SCH$_3$	0.76	1.89	1.70	0.81	0.63	0.72	0.15	-11.01
$\cdot$CF=CH$_2$	0.94	6.12	3.71	0.96	0.42	0.64	0.46	6.26
$\cdot$CH$_2$CH$_2$F	0.76	0.30	0.27	0.13	0.08	0.10	0.04	-1.53
$\cdot$CH$_2$CHO	0.93	5.01	2.86	0.32	-0.16	0.02	0.46	-10.11
$\cdot$CH$_2$CN	0.94	6.36	3.52	0.65	-0.02	0.21	0.46	-8.66
$\cdot$CH$_2$F	0.76	1.03	1.00	0.52	0.55	0.57	0.06	-4.22
$\cdot$CH$_2$NH$_2$	0.76	1.28	1.18	0.59	0.50	0.52	0.06	-12.06
$\cdot$CH$_2$NH$_3$$^+$	0.76	0.16	0.10	0.08	0.06	0.03	0.02	4.58
$\cdot$CH$_2$NHOH	0.77	1.76	1.57	0.78	0.58	0.64	0.15	-8.81
$\cdot$CH$_2$OH	0.76	1.29	1.23	0.62	0.57	0.60	0.07	-9.27
$\cdot$CH$_2$PH$_3$$^+$	0.76	0.21	0.14	0.01	0.01	-0.02	0.05	0.49
$\cdot$CH$_2$SH$_2$$^+$	0.77	0.41	0.30	0.12	0.11	0.08	0.06	2.29
$\cdot$CH$_2$SH	0.76	1.60	1.43	0.68	0.57	0.63	0.12	-9.68

$\dot{\text{R}}$	$\langle \hat{S}^2 \rangle_{\text{SCF}}$	ΔCEPA$_0$	ΔDC-12	ΔCCSD	ΔOCEPA$_0$	ΔODC-12	ΔCCSD(T)	CCSD(T)+δQ
$\dot{\text{C}}\text{H}_2\text{C}\equiv\text{CH}$	1.00	6.23	3.47	0.82	-0.03	0.23	0.52	-13.17
$\dot{\text{C}}\text{H}_2\text{CH}_3$	0.76	0.30	0.26	0.11	0.08	0.10	0.03	-3.36
$\dot{\text{C}}\text{H}_2\text{Cl}$	0.77	1.13	1.02	0.50	0.48	0.51	0.09	-5.67
$\dot{\text{C}}\text{H}_2\text{BH}_2$	0.76	0.17	0.17	0.05	0.03	0.04	0.05	-11.66
$\dot{\text{C}}\text{HO}$	0.77	2.26	2.24	1.48	1.55	1.56	0.20	-17.61
$\dot{\text{C}}\text{H}_2\text{PH}_2$	0.76	1.17	1.02	0.39	0.36	0.39	0.12	-6.50
$\dot{\text{C}}\text{HClF}$	0.76	1.61	1.52	0.76	0.78	0.81	0.13	-6.61
$\dot{\text{C}}\text{HFCH}_3$	0.76	1.07	1.01	0.50	0.51	0.53	0.08	-5.87
$\dot{\text{C}}\text{H(OH)}_2$	0.76	1.30	1.22	0.60	0.60	0.61	0.08	-6.67
$\dot{\text{C}}\text{HCl}_2$	0.77	1.78	1.57	0.72	0.72	0.75	0.15	-9.56
$\dot{\text{C}}\text{HF}_2$	0.76	1.50	1.48	0.78	0.83	0.85	0.10	-4.07
$\text{CH}_2=\dot{\text{C}}-\text{CN}$	1.39	19.10	11.50	2.36	-0.31	0.29	1.80	1.98
$\dot{\text{C}}\equiv\text{CH}$	1.15	11.20	6.51	0.77	-0.78	-0.07	0.82	26.25
$\dot{\text{C}}\text{H}=\text{CH}_2$	0.94	5.42	3.01	0.58	0.11	0.31	0.40	5.49
$\dot{\text{C}}\text{H}_2-\text{CH}=\text{CH}_2$	0.97	4.98	3.17	0.51	0.11	0.31	0.48	-17.53
		Δ_{MAE}:	2.97	2.01	0.62	0.40	0.43	0.25
		Δ_{SD}:	3.97	2.27	0.45	0.43	0.35	0.35

homodesmotic reaction

$$RH + {}^{\bullet}CH_3 \longrightarrow {}^{\bullet}R + CH_4 \tag{2.6}$$

where exothermic (negative) values indicate that the radical ${}^{\bullet}R$ is more thermo-dynamically stable than ${}^{\bullet}CH_3$.[64] For our benchmark we use the RSE30 dataset[62], which provides a diverse variety of ${}^{\bullet}R$ species (listed in table 2.3). Since the performance of CCSD(T) is known to deteriorate for strongly spin-contaminated UHF references,[65–69] we augment CCSD(T) energies with a quadruples correction ($\Delta Q = E_{\mathrm{CCSDT(Q)}} - E_{\mathrm{CCSD(T)}}$) and use these as our benchmark. CBS-extrapolated CCSD(T) reference values have been published for this dataset,[30] but we use CCSD(T) values computed with the cc-pCVTZ basis set to avoid basis-set incompleteness effects. The δQ correction was evaluated using the cc-pCVDZ basis set. As in the previous Section, DC-06 and ODC-06 computations cannot be converged for all database members and are omitted in the analysis below (see Supporting Information for incomplete DC-06 and ODC-06 data).

The relative performance of the DCFT, CEPA, and CC methods for the RSE30 dataset is shown in fig. 2.3. The effect of orbital-optimization on accuracy is now even more pronounced, reducing the large Δ_{MAE} errors of CEPA$_0$ (2.97 kcal mol^{-1}) and DC-12 (2.01 kcal mol^{-1}) to 0.40 and 0.43 kcal mol^{-1} for OCEPA$_0$ and ODC-12, respectively. CCSD has a slightly larger Δ_{MAE} value (0.62 kcal mol^{-1}), while CCSD(T) has the smallest overall Δ_{MAE} (0.25 kcal mol^{-1}). Both CEPA$_0$ and DC-12 show large standard deviations again (3.97 and 2.27 kcal mol^{-1}, respectively).

For OCEPA$_0$, the standard deviation (0.43 kcal mol^{-1}) is similar to that of CCSD (0.45 kcal mol^{-1}). ODC-12 and CCSD(T) exhibit the most consistent performance with the same Δ_{SD} value of 0.35 kcal mol^{-1}.

Deviations from CCSD(T)+δQ for individual RSEs predicted by each method are tabulated in table 2.3. In addition, table 2.3 includes expectation values of the square-norm spin operator computed for the UHF wavefunction of $\cdot$R ($\langle \hat{S}^2 \rangle_{\text{SCF}}$). The largest errors in computed RSEs were obtained for $\cdot$R species with $\langle \hat{S}^2 \rangle_{\text{SCF}} > 0.9\ \hbar^2$ (radicals 4, 6, 7, 16, and 27-30 in table 2.3). For these systems, the average CEPA$_0$ and DC-12 errors are 8.05 and 4.72 kcal mol^{-1}, and the average CCSD(T) error is 0.68 kcal mol^{-1}. OCEPA$_0$ and ODC-12 offer remarkably better performance for this subset, with average errors of 0.24 kcal mol^{-1} and 0.26 kcal mol^{-1}.

2.5.4 Adiabatic Ionization Energies in Electron-Dense Molecules

We conclude the assessment of DCFT methods for the description of thermodynamic properties by computing adiabatic ionization energies (AIEs) for a set of 10 di- and triatomic electron-dense molecules (table 2.4), i.e. those that are composed of elements with small atomic radius, high electron affinity, and high electronegativity (N, O, F), in order to increase the magnitude of electron correlation effects. We use experimentally measured ionization energies reported to high precision ($\sim$0.01 eV)[70–73] as reference values for our benchmark (IE$_{\text{ref}}$, table 2.4). The AIEs were computed using the cc-pCVQZ basis set, with harmonic ZPVE corrections applied to each neutral and cationic system.

Figure 2.3: Mean absolute deviations (Δ_{MAE}, kcal mol^{-1}) and the standard deviations from the mean signed error (Δ_{SD}, kcal mol^{-1}) of the radical stabilization energies (RSEs) for 30 open-shell doublet species (RSE30 database) computed using six methods with the cc-pCVTZ basis set. The errors are relative to CCSD(T) with an added quadruples correction ($\delta\mathrm{Q} = E_{\mathrm{CCSDT(Q)}} - E_{\mathrm{CCSD(T)}}$). The $\delta\mathrm{Q}$ correction was computed using the cc-pCVDZ basis set. RSE is defined as the reaction enthalpy for the homodesmotic reaction $^{\cdot}\mathrm{CH}_3 + \mathrm{RH} \rightarrow \mathrm{CH}_4 + {^{\cdot}}\mathrm{R}$. The Δ_{MAE} value is represented as a height of each colored box, while the Δ_{SD} value is depicted as a radius of the black vertical bar. See table 2.3 for data on individual database members.

22
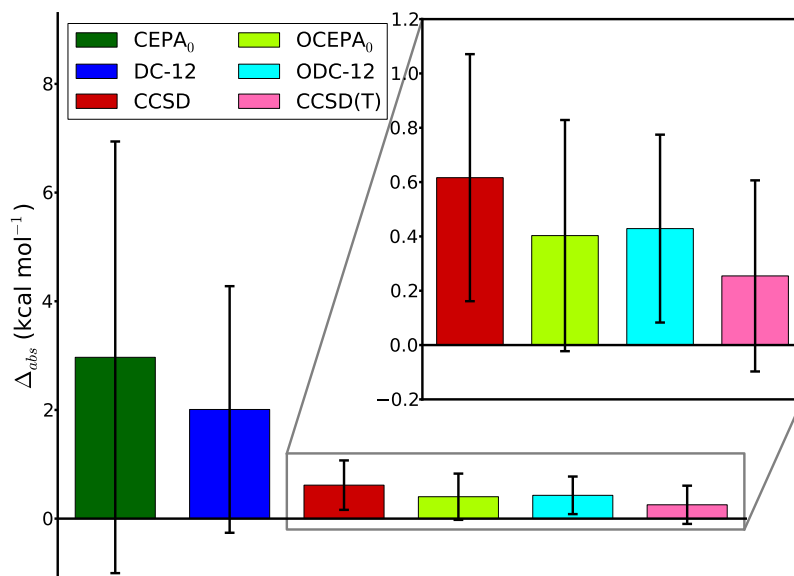
Table 2.4: Errors in adiabatic ionization energies (AIEs, eV) for 10 di- and triatomic molecules computed using six methods with the cc-pCVQZ basis set. The errors are relative to experimental values (IE_{ref}, eV) from Ref. 70, unless noted otherwise. For all AIEs the harmonic zero-point vibrational energy corrections were included. For each method the mean absolute deviations from IE_{ref} (Δ_{MAE}, eV) and the standard deviations from the mean signed error (Δ_{SD}, eV) are also shown.

Molecule	Transition	$\Delta CEPA_0$	ΔDC-12	$\Delta CCSD$	$\Delta OCEPA_0$	ΔODC-12	$\Delta CCSD(T)$	IE_{ref}
N_2	$^1\Sigma_g^+ \to {}^2\Sigma_g^+$	0.08	0.17	0.12	-0.05	0.07	-0.03	15.581 $\pm$ 0.008 [a]
O_2	$^3\Sigma_g^- \to {}^2\Pi_g$	-0.11	-0.03	0.04	-0.09	-0.02	-0.04	12.0697 $\pm$ 0.0002
F_2	$^1\Sigma_g^+ \to {}^2\Pi_g$	0.06	0.06	0.04	0.08	0.01	-0.03	15.697 $\pm$ 0.003
NO	$^2\Pi \to {}^1\Sigma^+$	-0.15	-0.05	-0.05	-0.05	-0.02	-0.09	9.26438 $\pm$ 0.00005
OF	$^2\Pi \to {}^3\Sigma^-$	0.11	0.12	-0.10	-0.03	-0.02	-0.11	12.77 $\pm$ 0.01 [b]
HNC	$^1\Sigma_g^+ \to {}^2\Sigma^+$	0.27	0.14	-0.12	-0.14	-0.08	-0.04	12.04 $\pm$ 0.01 [c]
HOF	$^1A' \to {}^2A''$	0.20	0.17	-0.10	-0.03	-0.04	-0.07	12.71 $\pm$ 0.01
FNO	$^1A' \to {}^2A''$	0.51	0.10	-0.02	-0.02	-0.00	0.04	12.63 $\pm$ 0.03
F_2N	$^2B_1 \to {}^1A_1$	0.07	0.10	0.07	0.01	0.03	-0.08	11.63 $\pm$ 0.01
F_2O	$^1A_1 \to {}^2B_1$	0.49	0.37	-0.01	0.05	0.04	-0.04	13.11 $\pm$ 0.01
	Δ_{MAE}:	0.21	0.13	0.06	0.05	0.03	0.06	
	Δ_{SD}:	0.22	0.12	0.08	0.06	0.04	0.04	

[a] Reference 71.

[b] Reference 72.

[c] Reference 73.

The Δ_{MAE} and Δ_{SD} values for our computed AIEs relative to experiment are plotted in fig. 2.4. Of the six methods, $CEPA_0$ and DC-12 exhibit the largest Δ_{MAE} values (0.21 and 0.13 eV, respectively). The closest agreement with experiment is given by ODC-12, with $\Delta_{\mathrm{MAE}} = 0.03$ eV. $OCEPA_0$, CCSD, and CCSD(T) show somewhat poorer performance ($\Delta_{\mathrm{MAE}} = 0.05$, 0.06 and 0.06 eV, respectively). The Δ_{SD} for ODC-12 matches that of CCSD(T) (0.04 eV). For the other methods, the Δ_{SD} values decrease in the order $CEPA_0$ (0.22 eV) > DC-12 (0.12) > CCSD (0.08) > $OCEPA_0$ (0.06).

Individual errors for each system are shown in table 2.4. Both DC-12 and $CEPA_0$ exhibit large deviations for F_2O (0.49 and 0.37 eV), and $CEPA_0$ also gives a large error for FNO (0.51 eV) which is the maximum error for this dataset. Both DC-12 and $CEPA_0$ give errors exceeding 0.1 eV for seven of the ten systems, whereas CCSD exhibits errors in excess of 0.1 eV for only three systems (OF, HNC, and HOF). CCSD(T) has only one such error (0.11 eV for OF), as does $OCEPA_0$ (0.14 eV for HNC). ODC-12 does the best of the methods considered, with a maximum error of 0.08 eV, found for the AIE of HNC.

2.5.5   Covalent Bond Stretching in Diatomic Molecules

Finally, we benchmark DCFT methods for covalent bond stretching. Although accurate description of bond stretching demands the use of multireference methods, our aim here is to explore the limits of DCFT away from equilibrium. For this purpose, we compute the energy as a function of bond distance for diatomic molecules with single (HF and BH), double (BeO), and triple (N_2) bonds using the

Figure 2.4: Mean absolute deviations (Δ_{MAE}, eV) and the standard deviations from the mean signed error (Δ_{SD}, eV) of adiabatic ionization energies for 10 di- and triatomic molecules computed using six methods with the cc-pCVQZ basis set. The errors are relative to experimental values.[70–73] The Δ_{MAE} value is represented as a height of each colored box, while the Δ_{SD} value is depicted as a radius of the black vertical bar. See table 2.4 for data on individual molecules.
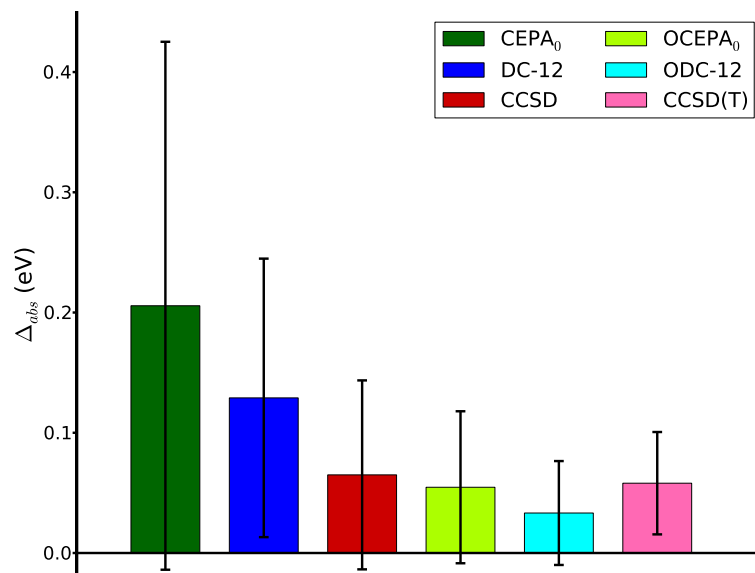
Figure 2.5: Error in the total energy $(\mathrm{m}E_{\mathrm{h}})$, relative to full CI, as a function of B–H internuclear separation (Å) computed using six methods with the DZP basis set. The full CI reference is depicted with a horizontal dotted line. The dashed vertical line indicates the full CI equilibrium bond distance.
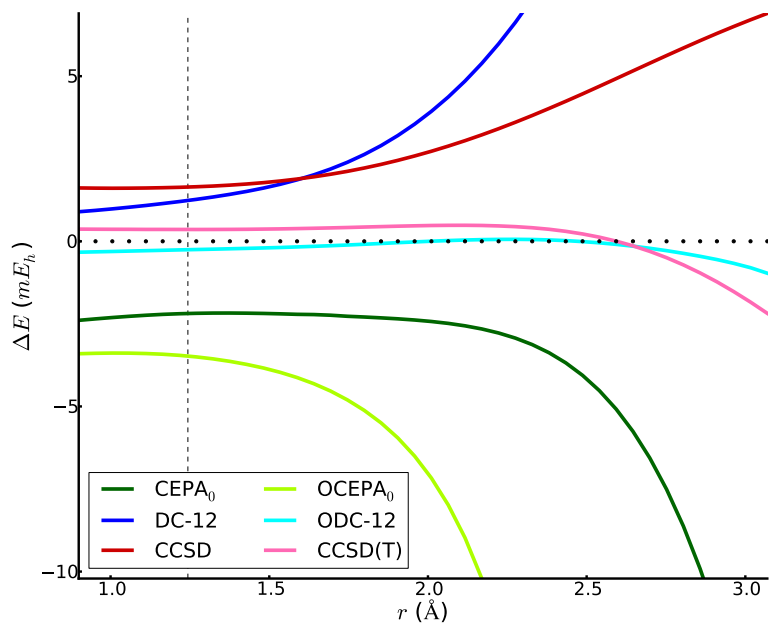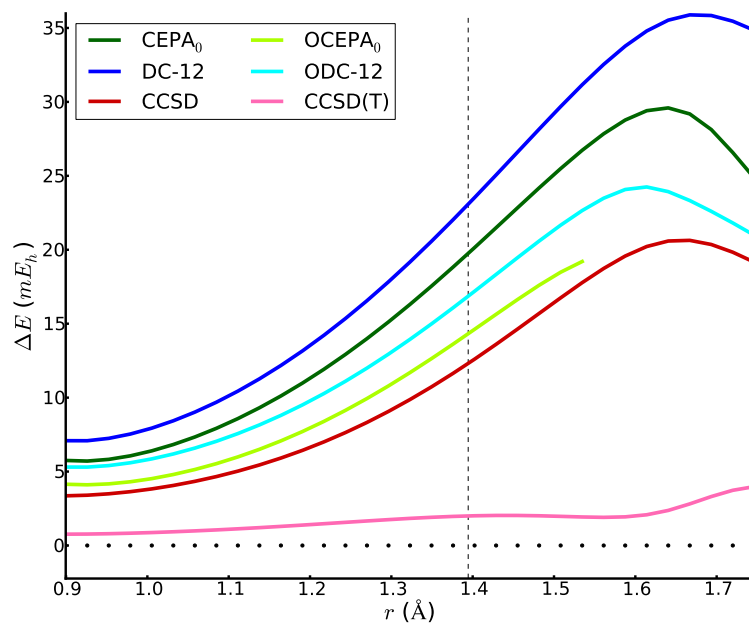
Figure 2.6: Error in the total energy (mE_h), relative to full CI, as a function of H–F internuclear separation (Å) computed using six methods with the DZP basis set. The full CI reference is depicted with a horizontal dotted line. The dashed vertical line indicates the full CI equilibrium bond distance.
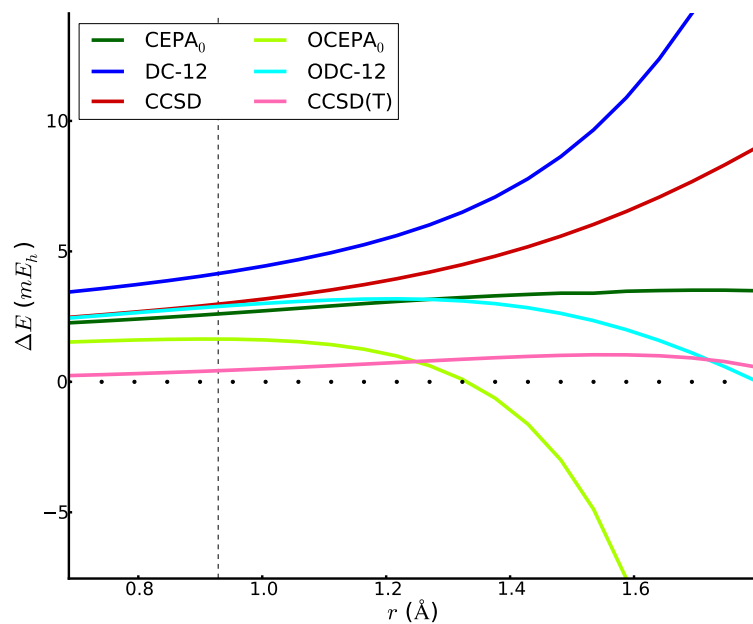
Figure 2.7:   Error in the total energy ($\mathrm{m}E_\mathrm{h}$), relative to full CI, as a function of Be–O internuclear separation (Å) computed using six methods with the 6-31G basis set. The full CI reference is depicted with a horizontal dotted line. The dashed vertical line indicates the full CI equilibrium bond distance.

Figure 2.8: Error in the total energy (mE_{h}), relative to full CI, as a function of N–N internuclear separation (Å) computed using six methods with the 6-31G basis set. The full CI reference is depicted with a horizontal dotted line. The dashed vertical line indicates the full CI equilibrium bond distance.

29
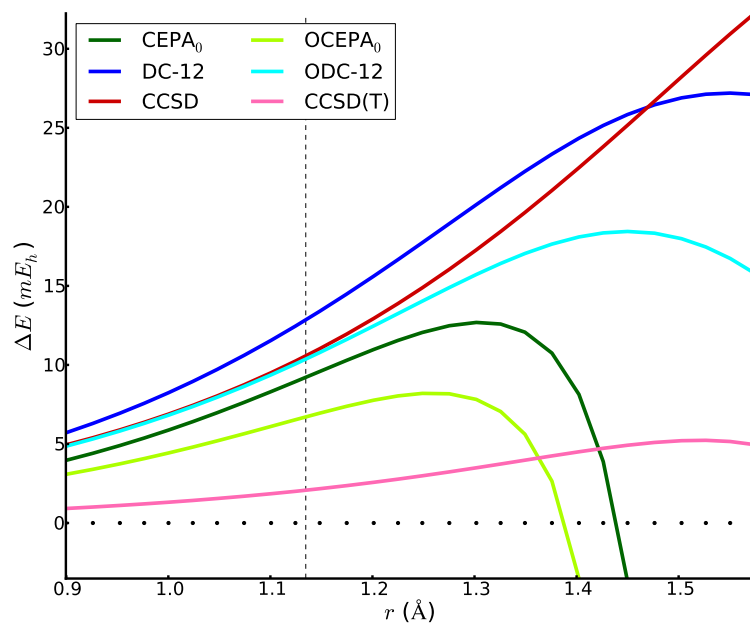
CEPA$_0$, OCEPA$_0$, DC-12, ODC-12, CCSD, and CCSD(T) methods. We restrict ourselves to modest basis sets in order to use full CI (FCI) as a reference, and plot the errors with respect to FCI (ΔE) as a function of internuclear distance for each molecule. The relative performance of the methods is described below using non-parallelity errors (NPE = $\Delta E_{\max} - \Delta E_{\min}$, m$E_\mathrm{h}$) computed for specific bond distance ranges.

BH Figure 2.5 shows errors relative to FCI for the BH molecule. DC-12 and CCSD increasingly overestimate the energy at larger internuclear distances, whereas the CEPA$_0$ error curve is concave down. Orbital optimization lowers the binding energy for OCEPA$_0$ even further compared to CEPA$_0$, leading to large errors with respect to FCI for r(B–H) ¿ 1.5 r_e, where r_e is the FCI equilibrium bond distance ($r_\mathrm{e} = 1.244$ Å). At 1.87 r_e, OCEPA$_0$ encounters convergence problems, which originate from numerical instabilities due to the method's deficiencies in the description of N-representability. The ODC-12 method exhibits much more stable behavior with respect to bond stretching in this case, fortuitously showing smaller errors and better parallelity than CCSD(T). For the range [0.72 r_e, 2.47 r_e], the NPEs decrease in the order DC-12 (24 mE_h) > CEPA$_0$ (15) > CCSD (5) > CCSD(T) (3) > ODC-12 (1).

HF Errors for HF bond stretching are plotted in fig. 2.6. The ΔE values of CCSD and DC-12 increase as a function of r(H–F), while CEPA$_0$ fortuitously maintains parallelity similar to CCSD(T) over the range [0.74 r_e, 1.94 r_e] ($r_\mathrm{e} = 0.929$ Å). OCEPA$_0$ increasingly overestimates the HF binding energy away from equilibrium,

30

failing to converge past 1.82 r_e. The ODC-12 method exhibits larger NPE than was observed for BH, and encounters convergence problems past 1.94 r_e. CCSD(T) shows the best overall performance, with errors between 0 and 1 mE_h. In the range [0.74 r_e, 1.94 r_e] the computed NPE values are: DC-12 (15 mE_h) > CCSD (7) > ODC-12 (3) > CEPA$_0$ (1) $\approx$ CCSD(T) (1). Recently, the orbital-optimized variants of CCSD(T) have been shown to yield good performance for HF bond stretching.[74]

BeO The double bond of BeO presents a more challenging test for the single-reference methods under consideration (fig. 2.7). All methods but CCSD(T) show qualitatively similar error curves, with inflection points near the FCI equilibrium (r_e = 1.394 Å) and valleys/peaks around 0.6 r_e/1.2 r_e. OCEPA$_0$ encounters convergence problems past 1.10 r_e. The ODC-12 method performs similarly to CCSD. Overall, the NPEs for the range [0.65 r_e, 1.10 r_e] decrease in the following order: DC-12 (29 mE_h) > CEPA$_0$ (24) > ODC-12 (19) > CCSD (17) > CCSD(T) (3).

N$_2$ Figure 2.8 depicts the errors relative to FCI for triple bond stretching in N$_2$. Here, OCEPA$_0$ fails to converge past 1.24 r_e (r_e = 1.135 Å). The ODC-12 method significantly overestimates the binding energy, possibly due to the lack of three-body correlation effects, but shows much more stable performance compared to methods other than CCSD(T). NPEs in the range [0.79 r_e, 1.39 r_e] decrease in the order: CEPA$_0$ (802 mE_h)[‡]> CCSD (27) > DC-12 (21) > ODC-12 (14) > CCSD(T) (4).

[‡]CEPA$_0$ exhibits a vertical asymptote at 1.36 r_e for N$_2$ stretching.

2.6   Conclusions

We have presented the benchmark study of four density cumulant functional theory (DCFT) methods (DC-06, DC-12, ODC-06, and ODC-12) developed recently in our group.[48;49;51;52] Specifically we have compared the performance of DCFT to that of coupled electron pair methods (CEPA$_0$ and OCEPA$_0$), as well as coupled-cluster theory [CCSD and CCSD(T)] for predicting a variety of chemical properties relevant to thermochemistry and kinetics, with a particular focus on open-shell, electron-dense, and non-equilibrium systems.

Our results indicate that among the four DCFT methods, the best agreement with available reference data is obtained for the ODC-12 method. While all four DCFT formulations yield similar results for the description of noncovalent interactions, DC-06, DC-12, and ODC-06 exhibit worse performance than ODC-12 for thermodynamic and kinetic properties of reactions involving open-shell molecules. In particular, DC-06 and ODC-06 frequently encounter convergence problems that originate from poor description of N-representability. In comparing ODC-12 to other methods, several trends can be observed:

(i) For all benchmark datasets, ODC-12 outperforms CCSD with errors smaller by almost a factor of two, on average. ODC-12 is also superior to CCSD for the description of single bond stretching in BH and HF, although it does not converge for all bond distances.

(ii) The performance of ODC-12 and OCEPA$_0$ is comparable. In particular, for hydrogen-transfer reaction barrier heights, the OCEPA$_0$ method yields smaller percent errors than ODC-12, whereas, for the radical stabilization energies (RSE)

and adiabatic ionization energies (AIE) in electron-dense molecules, the ODC-12 method smaller standard deviations than $OCEPA_0$. For AIEs, ODC-12 gives smaller mean absolute deviations by almost a factor of two. ODC-12 also shows significantly smaller non-parallelity errors than $OCEPA_0$ for covalent bond stretching, and can be converged for a larger range of distances for all diatomic molecules studied.

(iii) For the two most challenging datasets, RSE and AIE, the standard deviation of ODC-12 and CCSD(T) are similar. While CCSD(T) yields smaller mean absolute errors for the RSE database, the ODC-12 method significantly outperforms CCSD(T) for the AIE test case. However, for bond stretching ODC-12 is competitive with CCSD(T) only for the BH dissociation and shows worse results for other molecules.

Overall, the data presented herein indicates that the ODC-12 method can be used as an efficient $\mathcal{O}(n^6)$ alternative to CCSD, capable of predicting thermodynamic and kinetic quantities that are competitive in accuracy with the "gold-standard" $\mathcal{O}(n^7)$ CCSD(T). Although our current implementation of ODC-12 is far from optimal, the ODC-12 equations have reduced non-linearities compared to CCSD, which makes them more amenable to parallel implementation. The efficiency of ODC-12 can also greatly benefit from spin-adaptation,[41;75;76] local approximations,[33;77–79] and density fitting.[77;80–82] Another important advantage of ODC-12 over CCSD is its stationarity, which makes the computation of first-order properties and analytic gradients more efficient and easily accessible. In particular, ODC-12 has potential to be used for computing accurate response properties

which do not suffer from a lack of gauge-invariance.[83;84]

Chapter 3

Linear-Response Density Cumulant Theory for Excited States: First Implementation and Benchmark Calculations[*]

3.1 Abstract

We present a linear-response formulation of density cumulant functional theory (DCT) that provides accurate access to many electronic states. DCT expresses the electronic energy as a Hermitian, size-extensive, and stationary functional of the one-particle density matrix and the two-particle density cumulant. In the original DCT formulation only the information about a single electronic state (usually, the ground state) is obtained. In this research, we combine DCT with linear response theory to obtain information about many electronic states simultaneously. We discuss the derivation of linear-response DCT, present its implementation for the ODC-12 method (LR-ODC-12), and benchmark its performance against highly accurate equation-of-motion coupled cluster theory with up to full triple excitations (EOM-CCSDT). Our results for a set of small molecules demonstrate that LR-ODC-12 vertical excitation energies are in closer agreement with EOM-CCSDT

---

[*]A. V. Copan and A. Yu. Sokolov (to be submitted in J. Chem. Theory Comput).

than those obtained from equation-of-motion coupled cluster theory with up to double excitations (EOM-CCSD). In addition, we report a linear-response formulation of the orbital-optimized linearized coupled cluster theory with double excitations (LR-OLCCD), which we obtain by neglecting the non-linear terms in the LR-ODC-12 equations.

3.2   Introduction

Accurate simulation of excited electronic states remains one of the major challenges in modern electronic structure theory. *Ab initio* methods for excited states can be divided into single-reference and multi-reference categories, based on their ability to treat static electron correlation. Multi-reference methods can correctly describe static correlation in near-degenerate valence orbitals and electronic states with multiple-excitation character, but often lack accurate treatment of important dynamic correlation effects (e.g., multi-configurational self-consistent field or multi-reference perturbation theories)[85–94] or become very costly when the number of near-degenerate orbitals is large (e.g., multi-reference configuration interaction or coupled cluster theories).[95–107] Meanwhile, single-reference methods[20;22;108–120] often provide a compromise between the computational cost and accuracy, and can be used to reliably compute properties of molecules in low-lying electronic states near the equilibrium geometries. In these situations, single-reference equation-of-motion coupled cluster theory (EOM-CC)[20;22;110–113] is usually the method of choice, especially when high accuracy is desired.

The EOM-CC methods yield size-intensive excitation energies[115;116] and can be

systematically improved by increasing the excitation rank of the cluster operator in the exponential parametrization of the wavefunction. Although EOM-CC is usually formulated in the context of a similarity-transformed Hamiltonian, its excitation energies are equivalent to those obtained from linear-response coupled cluster theory (LR-CC).[114–116] Both EOM-CC and LR-CC are based on non-Hermitian eigenvalue problems, complicating the computation of molecular properties (e.g., transition dipoles) by requiring evaluation of left and right eigenvectors.[121–124] Several Hermitian alternatives to EOM-CC and LR-CC have been proposed to avoid these problems, such as algebraic diagrammatic construction[125–129], unitary and variational LR-CC,[130–132] similarity-constrained CC,[133] and propagator-based LR-CC.[134;135]

In this work, we present the development of linear-response density cumulant functional theory (LR-DCT), a size-intensive approach for excited electronic states. In density cumulant functional theory (DCT),[34;48;49;51;52;136;137] the electronic energy is obtained by optimizing the energy functional directly in terms of the one-particle reduced density matrix and the two-particle density cumulant, a fully connected part of the two-particle reduced density matrix (2-RDM).[38–41;43;47;138–141] In this regard, DCT is related to approaches that are based on the variational optimization[40;142–147] or parametrization[35–37] of 2-RDM. On the other hand, DCT has a close relationship[51;52] with wavefunction-based electronic structure theories, such as linearized, unitary, and variational coupled cluster theory.[4;148–155] In contrast to variational 2-RDM theory[44–46] and traditional coupled cluster methods [e.g., CCSD and CCSD(T)],[20;22] DCT naturally combines size-extensivity and a

Hermitian energy functional. In addition, the DCT electronic energy is fully relaxed with respect to all of its parameters, which greatly simplifies computation of the first-order molecular properties.[156–159] We have successfully applied DCT to a variety of chemical systems with different electronic structure effects (e.g., open-shell, symmetry-breaking, and multi-reference).[52;136;137;160;161] One limitation of the original DCT formulation is that it can only obtain information about the lowest-energy state of a particular symmetry (usually, the ground state). By combining DCT with linear response theory, we remove this limitation, providing access to many electronic states simultaneously.

We begin with a brief overview of DCT (section 3.3.1) and linear response theory (section 3.3.2). We then discuss the derivation of linear-response theory for the ODC-12 method (LR-ODC-12, section 3.3.3). In section section 3.3.4, we derive equations for the linear-response orbital-optimized linearized coupled cluster theory with double excitations (LR-OLCCD), which we obtain by neglecting the non-linear terms in the LR-ODC-12 equations. We outline the computational details in section 3.4. In section section 3.5, we demonstrate that the LR-ODC-12 excitation energies are size-intensive (section 3.5.1), test the performance of LR-ODC-12 for the dissociation of H_2 (section 3.5.2), and benchmark the accuracy of LR-ODC-12 for vertical excitation energies of small molecules (section 3.5.3). Finally, we present our conclusions in section section 3.6.

3.3   Theory

3.3.1   Overview of Density Cumulant Theory

We begin with a brief overview of DCT for a single electronic state. Our starting point is to express the electronic energy as a trace of the one- and antisymmetrized two-electron integrals (h_p^q and $\overline{g}_{pq}^{rs}$) with the reduced one- and two-body density matrices (γ_q^p and γ_{rs}^{pq}):

$$E = h_p^q \gamma_q^p + \tfrac{1}{4} \overline{g}_{pq}^{rs} \gamma_{rs}^{pq} \tag{3.1}$$

where summation over the repeated indices is implied. In DCT, the two-body density matrix γ_{rs}^{pq} is expanded in terms of its connected part, the two-body density cumulant (λ_{rs}^{pq}), and its disconnected part, which is given by an antisymmetrized product of one-body density matrices:[34]

$$\gamma_{rs}^{pq} = \langle \Psi | a_{rs}^{pq} | \Psi \rangle = \lambda_{rs}^{pq} + P_{(r/s)} \gamma_r^p \gamma_s^q \tag{3.2}$$

where $P_{(r/s)} v_{rs} = v_{rs} - v_{sr}$ denotes antisymmetrization and $a_{rs}^{pq} = a_p^\dagger a_q^\dagger a_s a_r$ is the two-body operator in second quantization. The one-body density matrix γ_q^p is determined from its non-linear relationship to the cumulant's partial trace:[51]

$$\gamma_q^p = \gamma_r^p \gamma_q^r - \lambda_{qr}^{pr} \tag{3.3}$$

This reduces eq. (3.1) to a functional of the two-body cumulant and the basis of spin-orbitals, thereby defining the DCT energy functional. The density cumulant

is parametrized by choosing a specific Ansatz for the wavefunction $|\Psi\rangle$ such that[136]

$$\lambda_{rs}^{pq} = \langle\Psi|a_{rs}^{pq}|\Psi\rangle_{\text{c}} \tag{3.4}$$

where c indicates that only fully connected terms are included in the parametrization. eq. (3.4) can be considered as a set of n-representability conditions that ensure that the resulting one- and two-electron density matrices represent a physical n-electron wavefunction. To compute the DCT energy, the functional (3.1) is made stationary with respect to all of its parameters. Importantly, due to the connected nature of eq. (3.4), DCT is both size-consistent and size-extensive for any parametrization of $|\Psi\rangle$, and is exact in the limit of a complete parametrization.[136]

In this work, we consider the ODC-12 method,[51;52] which parametrizes the cumulant through a unitary treatment of single excitations and a linear expansion of double excitations.

$$|\Psi\rangle = e^{T_1 - T_1^\dagger}(1 + \hat{T}_2)|\Phi\rangle \tag{3.5}$$

$$T_1 = \mathbf{t}_1 \cdot \mathbf{a}_1 = t_a^i a_i^a \tag{3.6}$$

$$T_2 = \mathbf{t}_2 \cdot \mathbf{a}_2 = \tfrac{1}{4}t_{ab}^{ij}a_{ij}^{ab} \tag{3.7}$$

(missing hats for the operators in many places. I generally prefer to keep hats in the equations) The exponential singles operator $e^{T_1 - T_1^\dagger}$ has the effect of a unitary transformation of the spin-orbital basis and is incorporated in our implementation of the ODC-12 method by optimizing the orbitals.[52] The $\mathbf{t}_1$ and $\mathbf{t}_2$ parameters are

obtained from the stationarity conditions

$$\frac{\partial E}{\partial \mathbf{t}_1^\dagger} \overset{!}{=} 0 \ , \qquad \frac{\partial E}{\partial \mathbf{t}_2^\dagger} \overset{!}{=} 0 \tag{3.8}$$

and are used to compute the ODC-12 energy. Explicit equations for the stationarity conditions are given in Refs. 51 and 52. Although in ODC-12 the wavefunction parametrization is linear with respect to double excitations (eq. (3.5)), the ODC-12 energy stationarity conditions are non-linear in $\mathbf{t}_2$ due to the non-linear relationship between the one-particle density matrix and the density cumulant (eq. (3.3)).[51] Neglecting the non-linear $\mathbf{t}_2$ terms in eq. (3.8) results in the equations that define the linearized orbital-optimized coupled cluster doubles method (OLCCD). This method is equivalent to the orbital-optimized coupled electron pair approximation zero (OCEPA$_0$).[29]

3.3.2 Linear Response Theory

We now briefly review linear response theory in the quasi-energy formulation.[162] The quasi-energy of a system perturbed by a time-dependent interaction $\hat{V} f(t)$ is defined as

$$Q(t) = \langle \Psi(t) | \hat{H} + \hat{V} f(t) - i \tfrac{\partial}{\partial t} | \Psi(t) \rangle \tag{3.9}$$

where $\Psi(t)$ is the phase-isolated wavefunction, from which the usual Schrödinger wavefunction can be recovered as $e^{-i \int_0^t dt' Q(t')} \Psi(t)$. Assuming that the perturbation is periodic

$$f(t) = \sum_\omega f(\omega) e^{-i\omega t} \tag{3.10}$$

the time average of the quasi-energy over a period of oscillation, denoted as $\{Q(t)\}$, is variational with respect to the exact dynamic state.[163] The independent parameters $\mathbf{u}(t)$ that define such a state can be written using a Fourier expansion

$$\mathbf{u}(t) = \sum_{n=0}^{\infty} \sum_{\omega_1\cdots\omega_n} \mathbf{u}(\omega_1,\ldots,\omega_n)e^{-i(\omega_1+\cdots+\omega_n)t} \tag{3.11}$$

where the outer sum runs over polynomial orders in $f(t)$. The stationarity of the time-averaged quasi-energy then implies the following relationship[164]

$$0 = \frac{d}{df(\omega)}\frac{\partial\{Q(t)\}}{\partial\mathbf{u}^\dagger(\omega)}\bigg|_{f=0} =$$

$$\frac{\partial^2\{Q(t)\}}{\partial\mathbf{u}^\dagger(\omega)\partial\mathbf{u}(\omega)}\frac{\partial\mathbf{u}(\omega)}{\partial f(\omega)}\bigg|_{f=0} + \frac{\partial^2\{Q(t)\}}{\partial\mathbf{u}^\dagger(\omega)\partial f(\omega)}\bigg|_{f=0} \tag{3.12}$$

which constitutes a linear equation for the first-order response of the system to the perturbation. When the frequency ω is in resonance with an excitation energy of the system, eq. (3.12) will result in an infinite first-order response $\dfrac{\partial\mathbf{u}(\omega)}{\partial f(\omega)}$. From eq. (3.12), we find that these poles occur when the Hessian matrix of the quasi-energy with respect to the wavefunction parameters $\mathbf{u}(\omega)$ becomes singular. We can express this Hessian matrix in the form

$$\frac{\partial^2\{Q(t)\}}{\partial\mathbf{u}^\dagger(\omega)\partial\mathbf{u}(\omega)}\bigg|_{f=0} \equiv \mathbf{E} - \omega\,\mathbf{M} \tag{3.13}$$

where $\mathbf{E}$ is the Hessian of the time-averaged electronic energy $\{\langle\Psi(t)|\hat{H}|\Psi(t)\rangle\}$ and $\omega\mathbf{M}$ is the Hessian of the time-derivative overlap $\{\langle\Psi(t)|i\dot{\Psi}(t)\rangle\}$. The excitation

energies of the system ω_k can therefore be determined by solving the following generalized eigenvalue equation:

$$\mathbf{E}\mathbf{z}_k = \omega_k\mathbf{M}\mathbf{z}_k \qquad (3.14)$$

where $\mathbf{M}$ serves as the metric matrix. eq. (3.14) allows the determination of excitation energies for an arbitrary parametrization of $|\Psi(t)\rangle$.

The generalized eigenvectors $\mathbf{z}_k$ can be used to compute transition properties for excited states. In particular, in the exact linear response theory[165] the transition strength of the perturbing interaction, $|\langle\Psi|\hat{V}|\Psi_k\rangle|^2$, is equal to the complex residue of the following quantity at $\omega \to \omega_k$:

$$\langle\langle\hat{V};\hat{V}\rangle\rangle_\omega \equiv \mathbf{v}'^\dagger \cdot \left.\frac{\partial\mathbf{u}(\omega)}{\partial f(\omega)}\right|_{f=0} \qquad (3.15)$$

This quantity is known as the linear response function and $\mathbf{v}'$ is termed the property gradient vector,[166] which is defined as follows:

$$\mathbf{v}' \equiv \left.\frac{\partial^2\{Q(t)\}}{\partial\mathbf{u}^\dagger(\omega)\partial f(\omega)}\right|_{f=0} \qquad (3.16)$$

Substituting eqs. (3.13) and (3.16) into eq. (3.12) and decomposing the quasi-energy Hessian as

$$\mathbf{E} - \omega\mathbf{M} = (\mathbf{Z}^\dagger)^{-1}(\mathbf{Z}^\dagger\mathbf{M}\mathbf{Z})(\mathbf{\Omega} - \omega\mathbf{1})(\mathbf{Z})^{-1} \qquad (3.17)$$

where $\mathbf{\Omega}$ is a diagonal matrix of generalized eigenvalues and $\mathbf{Z}$ is a matrix of

43

generalized eigenvectors that simulataneously diagonalizes $\mathbf{E}$ and $\mathbf{M}$, we obtain the general formula for the transition strengths:

$$\lim_{\omega \to \omega_k} (\omega - \omega_k) \langle\langle \hat{V}; \hat{V} \rangle\rangle_\omega = \frac{|\mathbf{z}_k^\dagger \mathbf{v}'|^2}{\mathbf{z}_k^\dagger \mathbf{M} \mathbf{z}_k} \tag{3.18}$$

In section 3.3.3, we will use the quasi-energy formalism to derive equations for the linear-response ODC-12 method (LR-ODC-12).

3.3.3 Linear-Response ODC-12

In the ODC-12 method, the electronic energy Hessian can be written in the following form

$$\mathbf{E} = \begin{pmatrix} \mathbf{A}_{11} & \mathbf{A}_{12} & \mathbf{B}_{11} & \mathbf{B}_{12} \\ \mathbf{A}_{21} & \mathbf{A}_{22} & \mathbf{B}_{21} & \mathbf{B}_{22} \\ \mathbf{B}_{11}^* & \mathbf{B}_{12}^* & \mathbf{A}_{11}^* & \mathbf{A}_{12}^* \\ \mathbf{B}_{21}^* & \mathbf{B}_{22}^* & \mathbf{A}_{21}^* & \mathbf{A}_{22}^* \end{pmatrix} \tag{3.19}$$

where the submatrices are defined in general as

$$\mathbf{A}_{nm} = \left. \frac{\partial^2 E}{\partial \mathbf{t}_n^\dagger \partial \mathbf{t}_m} \right|_{f=0}, \quad \mathbf{B}_{nm} = \left. \frac{\partial^2 E}{\partial \mathbf{t}_n^\dagger \partial \mathbf{t}_m^*} \right|_{f=0}. \tag{3.20}$$

These complex derivatives relate to the second derivatives of the electronic energy with respect to variations of the orbitals ($\mathbf{A}_{11}$, $\mathbf{B}_{11}$) and cumulant parameters ($\mathbf{A}_{22}$, $\mathbf{B}_{22}$). Similarly, the mixed second derivatives couple variations in the orbitals and cumulant parameters ($\mathbf{A}_{12}$, $\mathbf{B}_{12}$). The metric matrix $\mathbf{M}$ has a block-diagonal structure, as a consequence of the linear parametrization of the wavefunction in

44

eq. (3.5):

$$\mathbf{M} = \begin{pmatrix} \mathbf{S}_{11} & \mathbf{0} & \mathbf{0} & \mathbf{0} \\ \mathbf{0} & \mathbf{1}_2 & \mathbf{0} & \mathbf{0} \\ \mathbf{0} & \mathbf{0} & -\mathbf{S}_{11}^* & \mathbf{0} \\ \mathbf{0} & \mathbf{0} & \mathbf{0} & -\mathbf{1}_2 \end{pmatrix} \tag{3.21}$$

where $\mathbf{1}_2 = \langle \Phi | \mathbf{a}_2^\dagger \mathbf{a}_2 | \Phi \rangle$ is an identity matrix over the space of unique two-body excitations and the orbital metric is defined as follows:

$$\omega \mathbf{S}_{11} = \frac{\partial^2 \{ \langle \Psi(t) | i \dot{\Psi}(t) \rangle \}}{\partial \mathbf{t}_1^\dagger(\omega) \partial \mathbf{t}_1(\omega)} \Bigg|_{f=0} \tag{3.22}$$

Equations for all blocks of $\mathbf{E}$, $\mathbf{M}$, and the property gradient vector $\mathbf{v}'$ are shown explicitly in the Supporting Information. We note that, due to the Hermitian nature of the DCT energy functional (3.1), the ODC-12 energy Hessian $\mathbf{E}$ is always symmetric. As a result, in the absence of instabilities (i.e., as long as the Hessian is positive semi-definite), the LR-ODC-12 excitation energies are guaranteed to have real values.

To illustrate the derivation of the LR-ODC-12 energy Hessian, let us consider the diagonal two-body block of $\mathbf{E}$. Expressing the energy (3.1) using the cumulant expansion (3.2) and differentiating with respect to $\mathbf{t}_2$, we obtain:

$$\begin{aligned} \mathbf{A}_{22} = \frac{\partial^2 E}{\partial \mathbf{t}_2^\dagger \partial \mathbf{t}_2} &= f_p^q \frac{\partial^2 \gamma_q^p}{\partial \mathbf{t}_2^\dagger \partial \mathbf{t}_2} + \bar{g}_{pr}^{qs} \frac{\partial \gamma_q^p}{\partial \mathbf{t}_2^\dagger} \frac{\partial \gamma_s^r}{\partial \mathbf{t}_2} \\ &+ \tfrac{1}{4} \bar{g}_{pq}^{rs} \frac{\partial^2 \lambda_{rs}^{pq}}{\partial \mathbf{t}_2^\dagger \partial \mathbf{t}_2} \end{aligned} \tag{3.23}$$

where we have introduced the generalized Fock matrix $f_p^q \equiv h_p^q + \bar{g}_{pr}^{qs} \gamma_s^r$. The derivatives of the one-body density matrix can be expressed in terms of the derivatives of the density cumulant

$$\begin{aligned}
\mathbf{A}_{22} &= \mathcal{F}_p^q \frac{\partial^2 \lambda_{qt}^{pt}}{\partial \mathbf{t}_2^\dagger \partial \mathbf{t}_2} + \mathcal{G}_{pr}^{qs} \frac{\partial \lambda_{qt}^{pt}}{\partial \mathbf{t}_2^\dagger} \frac{\partial \lambda_{su}^{ru}}{\partial \mathbf{t}_2} \\
&\quad + \tfrac{1}{4} \bar{g}_{pq}^{rs} \frac{\partial^2 \lambda_{rs}^{pq}}{\partial \mathbf{t}_2^\dagger \partial \mathbf{t}_2}
\end{aligned}$$

(3.24)

where the intermediates $\mathcal{F}_p^q$ and $\mathcal{G}_{pr}^{qs}$ can be computed using a transformation of the one- and two-electron integrals to the natural spin-orbital basis (see section 3.A for details). These cumulant derivatives are straightforward to evaluate from eqs. (3.4) and (3.5) using either algebraic or diagrammatic techniques.

Next, let us outline the derivation of the one-body metric. Substituting eq. (3.5) into eq. (3.22) gives

$$\begin{aligned}
\omega \mathbf{S}_{11} &= \frac{1}{2} \frac{\partial^2 \{\langle \Psi | [i\dot{T}_1^\dagger(t), T_1(t)] | \Psi \rangle\}}{\partial \mathbf{t}_1^\dagger(\omega) \partial \mathbf{t}_1(\omega)} \bigg|_{f=0} \\
&\quad - \frac{1}{2} \frac{\partial^2 \{\langle \Psi | [T_1^\dagger(t), i\dot{T}_1(t)] | \Psi \rangle\}}{\partial \mathbf{t}_1^\dagger(\omega) \partial \mathbf{t}_1(\omega)} \bigg|_{f=0}
\end{aligned}$$

(3.25)

where we have assumed that we are working in the variational orbital basis so that $T_1(t)|_{f=0} = 0$, and $\Psi = \Psi(t)|_{f=0}$ denotes the ground state wavefunction. Using the Fourier expansion of the $\mathbf{t}_1(t)$ parameters (eq. (3.11)), the gradients of the time

46

derivatives can be evaluated as:

$$\left.\frac{\partial i \dot{T}_1^\dagger(t)}{\partial \mathbf{t}_1^\dagger(\omega)}\right|_{f=0} = -\omega \mathbf{a}_1^\dagger e^{+i\omega t} \tag{3.26}$$

$$\left.\frac{\partial i \dot{T}_1(t)}{\partial \mathbf{t}_1(\omega)}\right|_{f=0} = +\omega \mathbf{a}_1 e^{-i\omega t} \tag{3.27}$$

Substituting eqs. (3.26) and (3.27) into eq. (3.25) and evaluating the gradients of T_1 and $T_1^\dagger$ similarly gives the final working equation for the one-body metric:

$$\omega(\mathbf{S}_{11})_{ia,jb} = \omega \langle \Psi | [a_a^i, a_j^b] | \Psi \rangle$$
$$= \omega(\delta_a^b \gamma_j^i - \delta_j^i \gamma_a^b) \tag{3.28}$$

3.3.4 Linear-Response OLCCD

As we discussed in section 3.3.1, the orbital-optimized linearized coupled cluster doubles method (OLCCD) can be considered as an approximation to the ODC-12 method where all of the non-linear $\mathbf{t}_2$ terms are neglected. Similarly, we can formulate the linear-response OLCCD method (LR-OLCCD) by linearizing the LR-ODC-12 equations. This simplifies the expressions for the electronic Hessian blocks that involve the second derivatives with respect to $\mathbf{t}_2$. For example, for the $\mathbf{A}_{22}$ block, we obtain:

$$\mathbf{A}_{22} = (f_0)_i^j \frac{\partial^2 \lambda_{jr}^{ir}}{\partial \mathbf{t}_2^\dagger \partial \mathbf{t}_2} - (f_0)_a^b \frac{\partial^2 \lambda_{br}^{ar}}{\partial \mathbf{t}_2^\dagger \partial \mathbf{t}_2} + \frac{1}{4} \bar{g}_{pq}^{rs} \frac{\partial^2 \lambda_{rs}^{pq}}{\partial \mathbf{t}_2^\dagger \partial \mathbf{t}_2} \tag{3.29}$$

47

where $(f_0)_p^q = h_p^q + \bar{g}_{pi}^{qi}$ is the usual (mean-field) Fock operator. Comparing eq. (3.29) with eq. (3.24) from the LR-ODC-12 method, we observe that the former equation can be obtained from the latter by replacing the $\mathcal{F}_p^q$ intermediates with the mean-field Fock matrix elements and ignoring the term that depends on $\mathcal{G}_{pr}^{qs}$. These simplifications arise from the fact that the $\mathcal{F}_p^q$ and $\mathcal{G}_{pr}^{qs}$ intermediates contain high-order $\mathbf{t}_2$ contributions that are not included in the linearized LR-OLCCD formulation (see section 3.A and Ref. 51 for details). For the $\mathbf{B}_{22}$ block, we find that all of the Hessian elements are zero. A complete set of working equations for LR-OLCCD is given in the Supporting Information.

3.4   Computational Details

The LR-ODC-12 and LR-OLCCD methods were implemented as a standalone Python program, which was interfaced with PSI4[167] and PYSCF[168] to obtain the one- and two-electron integrals. To compute excitation energies, our implementation utilizes the multi-root Davidson algorithm,[169;170] which solves the generalized eigenvalue problem (3.14) by progressively growing an expansion space for the n_{root} lowest generalized eigenvectors of the electronic Hessian and the metric matrix. A key feature of this algorithm is that it avoids storing the Hessian and metric matrices, significantly reducing the amount of memory required by the computations. Our implementation of the energy Hessian was validated by computing the static response function for a dipole perturbation (i.e., the dipole polarizability):

$$\langle\langle \hat{V}; \hat{V} \rangle\rangle_0 = -\mathbf{v}'^\dagger \mathbf{E}^{-1} \mathbf{v}' \tag{3.30}$$

48

This quantity can also be evaluated numerically as a derivative of the ground state energy

$$\langle\langle \hat{V}; \hat{V} \rangle\rangle_0 = \left. \frac{d^2 E}{df^2} \right|_{f=0} \qquad (3.31)$$

by perturbing the one-electron integrals $h_p^q \leftarrow h_p^q + f \langle \psi_p | \hat{V} | \psi_q \rangle$ and solving the ODC-12 equations for different values of f.

We used Q-CHEM 4.4[171] to obtain results from equation-of-motion coupled cluster theory with single and double excitations (EOM-CCSD) and EOM-CCSD with triple excitations in the EOM part [EOM-CC(2,3)]. The MRCC program[172] was used to obtain results for equation-of-motion coupled cluster theory with up to full triple excitations (EOM-CCSDT). All electrons were correlated in all computations. We used tight convergence parameters in all ground-state (10^{-8} E_h) and excited-state computations (10^{-5} E_h). In sections 3.5.2 and 3.5.3, the augmented aug-cc-pVTZ and d-aug-cc-pVTZ basis sets of Dunning and co-workers were employed.[59] For alkenes (section 4.0.1), the ANO-L-pVXZ (X = D, T) basis sets[173] were used as in Ref. 174. To compute vertical excitation energies in section 3.5.3, geometries of molecules were optimized using ODC-12 (for LR-ODC-12), OLCCD (for LR-OLCCD), or CCSD [for EOM-CCSD, EOM-CC(2,3), and EOM-CCSDT]. For alkenes in section 4.0.1, the frozen-core MP2/cc-pVQZ geometries were used as in Refs. 174 and 175.

Table 3.1: Ground-state energies (in E_{h}) and vertical excitation energies (in eV) for the four lowest-energy excited states of the CO molecule and noninteracting systems of CO with Ne atoms (CO + nNe, n = 1, 2, 3) computed using the ODC-12 and LR-ODC-12 methods (cc-pVDZ basis set). The noninteracting systems were separated from each other by 10000 Å and the C–O bond distance was set to 1.12547 Å. Results demonstrate size-intensivity of the LR-ODC-12 excitation energies.

	CO	CO + Ne	CO + 2Ne	CO + 3Ne
$X\,^1\Sigma_g^+$	-113.051282	-241.730913	-370.410543	-499.090174
$^3\Pi$	6.48596	6.48596	6.48596	6.48596
$^3\Sigma^+$	8.41225	8.41225	8.41225	8.41225
$^1\Pi$	8.90866	8.90866	8.90866	8.90866
$^3\Delta$	9.33189	9.33189	9.33189	9.33189

3.5 Results

3.5.1 Size-Intensivity of the LR-ODC-12 Energies

In section 3.3.1, we discussed that all DCT methods are by construction *size-extensive*, meaning that their electronic energies scale linearly with the number of electrons. In this section, we demonstrate that the LR-ODC-12 excitation energies are *size-intensive*, i.e. they satisfy the following property: $E(A^* + B) = E(A^*) + E(B)$, where A and B are two noninteracting fragments in their corresponding ground states and A^* is the fragment A in an excited state. table 3.1 shows the ODC-12 ground-state energies and the LR-ODC-12 excitation energies for the CO molecule and noninteracting systems composed of CO and the neon atoms separated by 10000 Å (CO + nNe, n = 1, 2, 3). The scaling of the ODC-12

energies for the ground $X\,^1\Sigma_g^+$ electronic state is perfectly linear up to $10^{-8}\ E_{\mathrm{h}}$, which is the convergence parameter used in our ODC-12 computations. Upon the addition of the neon atoms, the excitation energies of the CO molecule remain constant up to the convergence threshold set in LR-ODC-12 (10^{-6} eV). These results provide numerical evidence that the LR-ODC-12 excitation energies are size-intensive.
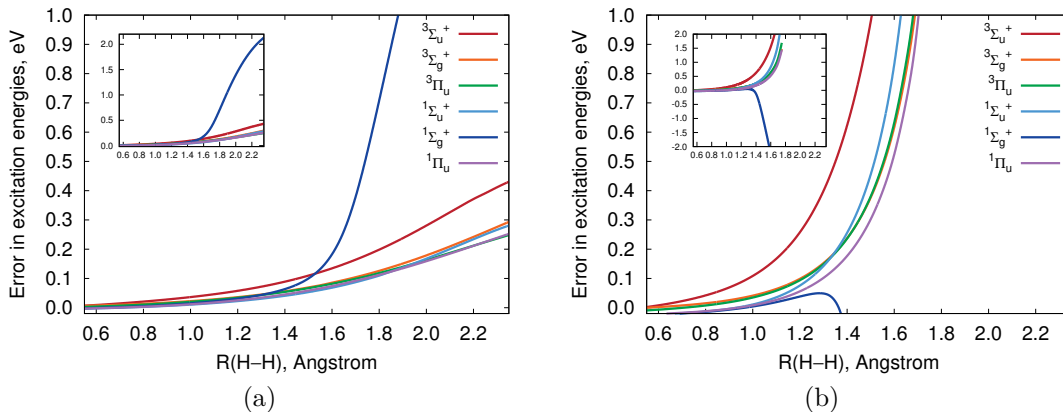
3.5.2 H_2 Dissociation

Figure 3.1: Errors in vertical excitation energies (eV) for six lowest-lying electronic states of H_2 computed using LR-ODC-12 (3.1a) and LR-OLCCD (3.1b) as a function of the H–H bond length, relative to full configuration interaction. All methods employed the d-aug-cc-pvtz basis set. In each figure, the inset shows the same plot for a larger range of errors.

One of the desirable properties of an electronic structure method is exactness for two-electron systems. While the ODC-12 method is not exact for two-electron systems, it has been shown to provide a very good description of the ground-state H_2 dissociation curve, with errors of ~ 1 kcal mol^{-1} with respect to full configuration interaction (FCI) near the dissociation limit.[52] Here, we investigate the

51

performance of LR-ODC-12 for the excited states of H_2. fig. 3.1a shows the errors in vertical excitation energies for six lowest-lying electronic states as a function of the H−H distance, relative to FCI. The FCI energies were computed using the EOM-CCSD method, which is exact for two-electron systems. At the equilibrium geometry ($r_e = 0.742$ Å) the errors in excitation energies for all states do not exceed 0.02 eV. Between 0.6 and 1.45 Å ($r \approx 2r_e$), the LR-ODC-12 excitation energies remain to be in a good agreement with FCI, with errors less than 0.1 eV for all states. In this range, the largest error is observed for the $^3\Sigma_u^+$ state. For $r \geq$ 1.5 Å, the error in the $^1\Sigma_g^+$ excited state energy rapidly increases from 0.10 eV (at 1.5 Å) to 2.13 eV (at 2.35 Å), while for other states the errors increase much more slowly. Analysis of the FCI wavefunction for the $^1\Sigma_g^+$ state shows a significant contribution from the $(1\sigma_g)^2 \rightarrow (1\sigma_u)^2$ double excitation already at $r = 1.55$ Å. This contribution becomes dominant for $r \geq 1.75$ Å. Thus, the large LR-ODC-12 errors observed for the $^1\Sigma_g^+$ state are likely due to the double-excitation character of this electronic state at long H−H bond distances. The second largest error near the dissociation is observed for the $^3\Sigma_u^+$ state (0.43 eV). For other electronic states, smaller errors of ~ 0.25 eV are observed near the dissociation.

We now compare the performance of LR-ODC-12 to that of the LR-OLCCD method, which can be considered as an approximation to LR-ODC-12 where all of the non-linear terms are removed in the description of electron correlation. fig. 3.1b shows the errors in the LR-OLCCD vertical excitation energies as a function of the H−H bond length. Although near the equilibrium geometry the performance of LR-OLCCD and LR-ODC-12 is similar, the LR-OLCCD errors increase much

Figure 3.2: Mean absolute errors. (provide more description)
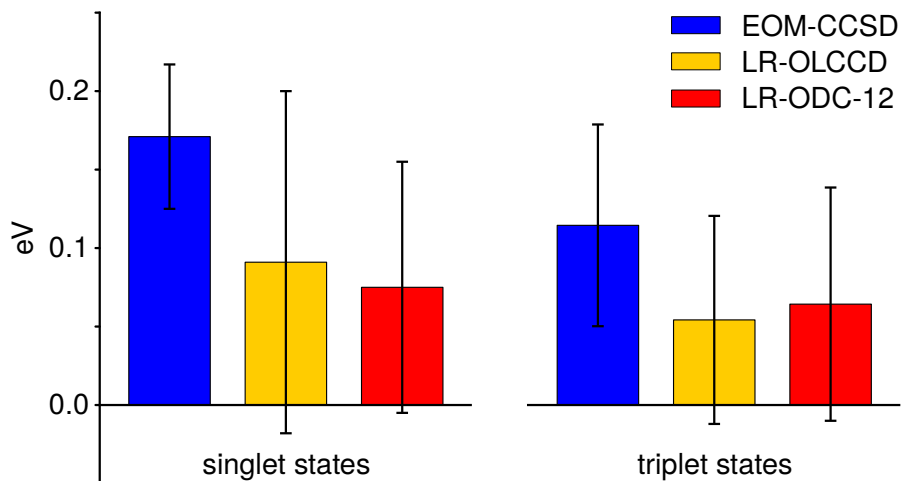
faster with increasing H−H distance compared to LR-ODC-12. At $r = 1.3$ Å, the LR-OLCCD error for the ${}^3\Sigma_u^+$ state (0.4 eV) is almost six times larger than the corresponding error from LR-ODC-12 (0.07 eV). For $r \geq 1.35$ Å, the LR-OLCCD errors for all excitation energies show very steep increase in magnitude, ranging from 1.5 to 4.7 eV already at $r = 1.75$ Å. We were unable to converge the LR-OLCCD equations for $r \geq 1.80$ Å. Overall, our results demonstrate that the non-linear terms in LR-ODC-12 significantly improve the description of excited states at long H−H distances when the electron correlation effects become particularly strong.

3.5.3 Benchmark: Small Molecules

Here we investigate the performance of our method for vertical excitation energies in several small molecules: N_2, CO, HCN, HNC, H_2C_2, and H_2CO. The refer-

Table 3.2: Errors in vertical excitation energies (eV) for singlet states computed using LR-OLCCD, LR-ODC-12, and EOM-CCSD, relative to EOM-CCSDT (aug-cc-pVTZ basis set). All electrons were correlated in all computations. Also shown are mean absolute errors (Δ_{MAE}) and standard deviations (Δ_{SD}) computed for each method.

		ΔEOM-CCSD	ΔLR-OLCCD	ΔLR-ODC-12	EOM-CCSDT
N_2	$^1\Pi_g$	0.18	0.08	0.20	9.29
	$^1\Sigma_u^-$	0.23	0.15	0.09	9.84
	$^1\Delta_u$	0.26	0.14	0.10	10.26
CO	$^1\Pi$	0.16	0.09	0.17	8.46
	$^1\Sigma^-$	0.19	-0.10	-0.01	9.89
	$^1\Delta$	0.19	-0.22	-0.05	10.03
HCN	$^1\Sigma^-$	0.16	0.05	0.00	8.25
	$^1\Delta$	0.17	0.04	0.01	8.61
	$^1\Pi$	0.17	0.05	0.20	9.12
HNC	$^1\Pi$	0.15	-0.01	0.10	8.13
	$^1\Sigma^+$	0.24	0.05	0.12	8.46
	$^1\Sigma^-$	0.15	-0.09	0.04	8.67
	$^1\Delta$	0.15	-0.18	-0.03	8.84
H_2C_2	$^1\Sigma_u^-$	0.12	0.06	0.02	7.11
	$^1\Delta_u$	0.10	0.07	0.03	7.45
H_2CO	$^1A_2$	0.10	-0.07	0.02	3.95
Δ_{MAE}		0.09	0.08	0.17	
Δ_{SD}		0.11	0.08	0.05	

ence values have been computed with EOM-CCSDT and we compare all-electron calculations with the same aug-cc-pVTZ basis in order to exclude basis set incompleteness error from the comparison. As an aggregate measure of the tendency for each method to deviate from the reference values, we calculate their mean absolute errors (Δ_{MAE}). As a measure of the degree to which the errors are systematically clustered above or below the reference values, we look at their standard deviation

from the average signed error (Δ_{SD}).

For the singlets, LR-ODC-12 has errors above 0.15 eV for three states, with a maximum error of 0.20 eV. All three of these occur for $^1\Pi$ states of linear molecules, which are dominated by $\sigma \rightarrow \pi^*$ excitations. EOM-CCSD has eleven errors greater than 0.15 eV, with a maximum error of 0.26 eV and no predictable pattern – the largest three errors occur for three qualitatively unrelated states: $^1\Delta$, $^1\Sigma^-$, and $^1\Sigma^+$. Interestingly, the EOM-CCSD errors are relatively tightly clustered around their mean error of 0.17 eV, with a standard deviation of 0.05 eV compared to 0.08 eV for LR-OCD-12. For the triplets, LR-ODC-12 has no errors at all above 0.15 eV, whereas EOM-CCSD has six, with a maximum error of 0.28 eV for the $^3\Sigma_u^-$ state of N_2. Here the EOM-CCSD description of $^3\Sigma^-$ states is consistently poor, but some of the larger errors occur for $^3\Sigma^+$ and $^3\Delta$ states as well. In aggregate, we see that LR-ODC-12 cuts the mean absolute errors of EOM-CCSD roughly in half for both singlet and triplet states. Notably, whereas the EOM-CCSD errors are exclusively positive, the LR-ODC-12 errors are more centered on 0 eV, suggesting a more balanced treatment of the ground and excited states.

Comparing LR-ODC-12 to LR-OLCCD we see that most of the errors are within 0.1 eV of each other, suggesting that the non-linear terms are relatively unimportant for many of these states. Significant differences occur for the $^1\Delta$ states of CO and HCN, where LR-OLCCD shows some deterioration, and for the $^1\Pi$ state of HCN, where the linearization leads to a significant error cancellation.

3.6 Conclusions

Our conclusions.

3.A Differentiating the One-Body Density in Density Cumulant Theory

Repeated differentiation of the one-body n-representability condition in DCT (eq. (3.3)) gives the following formulas for first and second derivatives of the cumulant trace.

$$\frac{\partial \lambda_{qr}^{pr}}{\partial y} = \gamma_s^p \frac{\partial \gamma_q^s}{\partial y} + \frac{\partial \gamma_s^p}{\partial y} \gamma_q^s - \frac{\partial \gamma_q^p}{\partial y} \tag{3.32}$$

$$\frac{\partial^2 \lambda_{qr}^{pr}}{\partial x \partial y} = \gamma_s^p \frac{\partial \gamma_q^s}{\partial x \partial y} + \frac{\partial \gamma_s^p}{\partial x \partial y} \gamma_q^s - \frac{\partial \gamma_q^p}{\partial x \partial y} \\ + \frac{\partial \gamma_s^p}{\partial x} \frac{\partial \gamma_q^s}{\partial y} + \frac{\partial \gamma_q^s}{\partial x} \frac{\partial \gamma_s^p}{\partial y} \tag{3.33}$$

In the natural spin-orbital basis (NSO, denoted by prime indices), where the one-body density matrix is diagonal, we can invert these equations to determine the first and second derivatives derivatives of the one-body density from the cumulant derivatives.

$$\frac{\partial \gamma_{q'}^{p'}}{\partial y} = \theta_{p'q'} \frac{\partial \lambda_{q'r}^{p'r}}{\partial y} \tag{3.34}$$

$$\frac{\partial^2 \gamma_{q'}^{p'}}{\partial x \partial y} = \theta_{p'q'} \frac{\partial^2 \lambda_{q'r}^{p'r}}{\partial x \partial y} - \delta_{r'}^{s'} \theta_{p'q'} \theta_{p's'} \theta_{q'r'} \frac{\partial \lambda_{s't}^{p't}}{\partial x} \frac{\partial \lambda_{q'u}^{r'u}}{\partial y} \\ - \delta_{r'}^{s'} \theta_{p'q'} \theta_{p's'} \theta_{q'r'} \frac{\partial \lambda_{q'u}^{r'u}}{\partial x} \frac{\partial \lambda_{s't}^{p't}}{\partial y} \tag{3.35}$$

56

Here we have defined the following matrix

$$\theta_{p'q'} \equiv \begin{cases} (\gamma_{p'} + \gamma_{q'} - 1)^{-1} & \text{if } p, q \in \text{occ} \\ & \text{or } p, q \in \text{vir} \\ 0 & \text{otherwise} \end{cases} \tag{3.36}$$

where $\gamma_{p'}$ denotes an eigenvalue of the one-body density matrix (i.e. an occupation number). Substituting eqs. (3.34) and (3.35) into the two-body energy Hessian in eq. (3.23) and simplifying allows us to determine the intermediates in eq. (3.24). In the NSO basis they are given by

$$\mathcal{F}_{p'}^{q'} \equiv \theta_{p'q'} f_{p'}^{q'} \tag{3.37}$$

$$\mathcal{G}_{p'r'}^{q's'} \equiv \theta_{p'q'}\theta_{r's'}(\bar{g}_{p'r'}^{q's'} - \mathcal{F}_{p'}^{s'}\delta_{r'}^{q'} - \mathcal{F}_{r'}^{q'}\delta_{p'}^{s'}) \tag{3.38}$$

but note that these quantities must be back-transformed to the variatonal orbital basis to be compatible with the other quantities in eq. (3.23).

3.B   Working equations for LR-ODC-12

3.B.1   Blocks of the Energy Hessian

$$(\mathbf{A}_{11})_{ia,jb} = h_j^i \gamma_a^b + h_a^b \gamma_j^i - (\bar{\mathbf{F}})_j^i \delta_a^b - (\bar{\mathbf{F}})_a^b \delta_j^i + \bar{g}_{nj}^{mi} \gamma_{ma}^{nb} + \bar{g}_{ma}^{nb} \gamma_{nj}^{mi} + \bar{g}_{jf}^{ie} \gamma_{ae}^{bf} + \bar{g}_{ae}^{bf} \gamma_{jf}^{ie}$$
$$+ \bar{g}_{me}^{ib} \gamma_{ja}^{me} + \bar{g}_{ja}^{me} \gamma_{me}^{ib}$$
$$\tag{3.39}$$

$$\bar{\mathbf{F}} \equiv \tfrac{1}{2}(\mathbf{F} + \mathbf{F}^\dagger) \qquad (\mathbf{F})_p^q \equiv h_p^t \gamma_t^q + \tfrac{1}{2}\bar{g}_{pt}^{uv}\gamma_{uv}^{qt} \tag{3.40}$$

$$(\mathbf{B}_{11})_{ia,jb} = \bar{g}_{be}^{im}\gamma_{ma}^{je} + \bar{g}_{ma}^{je}\gamma_{be}^{im} + \bar{g}_{mb}^{ie}\gamma_{ae}^{jm} + \bar{g}_{ae}^{jm}\gamma_{mb}^{ie} + \tfrac{1}{2}\bar{g}_{mn}^{ij}\gamma_{ab}^{mn} + \tfrac{1}{2}\bar{g}_{ab}^{mn}\gamma_{mn}^{ij}$$

$$+\tfrac{1}{2}\bar{g}_{ef}^{ij}\gamma_{ab}^{ef} + \tfrac{1}{2}\bar{g}_{ab}^{ef}\gamma_{ef}^{ij}$$

$$\tag{3.41}$$

$$(\mathbf{A}_{22})_{ijab,klcd} = -P_{(a/b|k/l)}^{(c/d)}\mathcal{F}_a^c\delta_b^d\delta_k^i\delta_l^j - P_{(k/l)}^{(i/j|c/d)}\mathcal{F}_k^i\delta_l^j\delta_a^c\delta_b^d + P_{(k/l)}\bar{g}_{ab}^{cd}\delta_k^i\delta_l^j + P^{(c/d)}\bar{g}_{kl}^{ij}\delta_a^c\delta_b^d$$

$$-P_{(a/b|k/l)}^{(i/j|c/d)}\bar{g}_{la}^{jc}\delta_b^d\delta_k^i + P_{(a/b)}^{(c/d)}\mathcal{G}_{af}^{ec}t_{eb}^{ij}t_{kl}^{fd*} + P_{(a/b|k/l)}\mathcal{G}_{ka}^{me}t_{eb}^{ij}t_{ml}^{cd*}$$

$$+P^{(i/j|c/d)}\mathcal{G}_{me}^{ic}t_{ab}^{mj}t_{kl}^{ed*} + P_{(k/l)}^{(i/j)}\mathcal{G}_{mk}^{in}t_{ab}^{mj}t_{nl}^{cd*}$$

$$\tag{3.42}$$

$$\mathcal{F}_{p'}^{q'} \equiv \theta_{p'q'}f_{p'}^{q'} \qquad \mathcal{G}_{p'r'}^{q's'} \equiv \theta_{p'q'}\theta_{r's'}(\bar{g}_{p'r'}^{q's'} - \mathcal{F}_{p'}^{s'}\delta_{r'}^{q'} - \mathcal{F}_{r'}^{q'}\delta_{p'}^{s'}) \tag{3.43}$$

$$\theta_{p'q'} \equiv \begin{cases} (\gamma_{p'} + \gamma_{q'} - 1)^{-1} & \text{if } p,q \in \text{occ} \\ & \text{or } p,q \in \text{vir} \\ 0 & \text{otherwise} \end{cases} \tag{3.44}$$

$$(\mathbf{B}_{22})_{ijab,klcd} = P_{(a/b|c/d)}\mathcal{G}_{ac}^{ef}t_{eb}^{ij}t_{fd}^{kl} + P_{(a/b)}^{(k/l)}\mathcal{G}_{na}^{ke}t_{eb}^{ij}t_{cd}^{nl} + P_{(c/d)}^{(i/j)}\mathcal{G}_{mc}^{if}t_{ab}^{mj}t_{fd}^{kl}$$

$$+P^{(i/j|k/l)}\mathcal{G}_{mn}^{ik}t_{ab}^{mj}t_{cd}^{nl} \tag{3.45}$$

$$(\mathbf{A}_{12})_{ia,klcd} = P_{(k/l)}\bar{g}_{la}^{cd}\delta_k^i + P^{(c/d)}\bar{g}_{kl}^{id}\delta_a^c + P_{(k/l)}(\mathcal{I}_a^i)_k^m t_{ml}^{cd*} + P^{(c/d)}(\mathcal{I}_a^i)_e^c t_{kl}^{ed*}$$

$$+P_{(k/l)}^{(c/d)}\bar{g}_{ae}^{mc}t_{ml}^{ed*}\delta_k^i + P_{(k/l)}^{(c/d)}\bar{g}_{ke}^{im}t_{ml}^{ed*}\delta_a^c + \tfrac{1}{2}P_{(k/l)}\bar{g}_{la}^{mn}t_{mn}^{cd*}\delta_k^i + \tfrac{1}{2}P^{(c/d)}\bar{g}_{ef}^{id}t_{kl}^{ef*}\delta_a^c \tag{3.46}$$

$$(\mathbf{B}_{12})_{ia,klcd} = P^{(k/l)}(\mathcal{I}_a^i)_m^k t_{cd}^{ml} + P_{(c/d)}(\mathcal{I}_a^i)_c^e t_{ed}^{kl} + P_{(c/d)}^{(k/l)}\bar{g}_{ad}^{le}t_{ce}^{ki} + P_{(c/d)}^{(k/l)}\bar{g}_{md}^{il}t_{ca}^{km} + \bar{g}_{ma}^{kl}t_{cd}^{im}$$

$$+\bar{g}_{cd}^{ie}t_{ae}^{kl} \tag{3.47}$$

$$(\mathcal{I}_a^i)_{k'}^{l'} \equiv \theta_{k'l'}(I_a^i)_{k'}^{l'} \qquad (I_a^i)_k^l \equiv +f_a^l\delta_k^i - \bar{g}_{ka}^{ml}\gamma_m^i + \bar{g}_{ke}^{il}\gamma_a^e \tag{3.48}$$

$$(\mathcal{I}_a^i)_{c'}^{d'} \equiv \theta_{c'd'}(I_a^i)_{c'}^{d'} \qquad (I_a^i)_c^d \equiv -f_c^i\delta_a^d + \bar{g}_{ac}^{md}\gamma_m^i - \bar{g}_{ec}^{id}\gamma_a^e \tag{3.49}$$

3.B.2 Blocks of the Metric Matrix

$$(\mathbf{S}_{11})_{ia,jb} = (\delta_a^b\gamma_j^i - \delta_j^i\gamma_a^b) \tag{3.50}$$

3.B.3 Blocks of the Property Gradient Vector

$$(\mathbf{p}_1)_{ia} = v_a^k\gamma_k^i - v_c^i\gamma_a^c \tag{3.51}$$

$$v_p^q \equiv \langle\psi_p|\hat{V}|\psi_q\rangle \tag{3.52}$$

$$(\mathbf{p}_2)_{ijab} = -P_{(a/b)}\mathcal{V}_a^e t_{eb}^{ij} - P^{(i/j)}\mathcal{V}_m^i t_{ab}^{mj} \tag{3.53}$$

$$\mathcal{V}_{p'}^{q'} \equiv \theta_{p'q'} v_{p'}^{q'} \tag{3.54}$$

3.C   Working Equations for LR-OLCCD

3.C.1   Blocks of the Energy Hessian

$$(\mathbf{A}_{11})_{ia,jb} = \text{Equation (3.39) with OLCCD density matrices.} \tag{3.55}$$

$$(\mathbf{B}_{11})_{ia,jb} = \text{Equation (3.41) with OLCCD density matrices.} \tag{3.56}$$

$$(\mathbf{A}_{22})_{ijab,klcd} = P_{(a/b|k/l)}^{(c/d)}(\mathbf{f}_0)_a^c \delta_b^d \delta_k^i \delta_l^j - P_{(k/l)}^{(i/j|c/d)}(\mathbf{f}_0)_k^i \delta_l^j \delta_a^c \delta_b^d + P_{(k/l)}\overline{g}_{ab}^{cd}\delta_k^i \delta_l^j$$
$$+ P^{(c/d)}\overline{g}_{kl}^{ij}\delta_a^c \delta_b^d - P_{(a/b|k/l)}^{(i/j|c/d)}\overline{g}_{la}^{jc}\delta_b^d \delta_k^i \tag{3.57}$$

$$(\mathbf{f}_0)_p^q = h_p^q + \overline{g}_{pi}^{qi} \tag{3.58}$$

$$(\mathbf{B}_{22})_{ijab,klcd} = 0 \tag{3.59}$$

$$(\mathbf{A}_{12})_{ia,klcd} = P_{(k/l)}\overline{g}_{la}^{cd}\delta_k^i + P^{(c/d)}\overline{g}_{kl}^{id}\delta_a^c + P_{(k/l)}(I_a^i)_k^m t_{ml}^{cd*} - P^{(c/d)}(I_a^i)_e^c t_{kl}^{ed*}$$

$$+P_{(k/l)}^{(c/d)}\overline{g}_{ae}^{mc}t_{ml}^{ed*}\delta_k^i + P_{(k/l)}^{(c/d)}\overline{g}_{ke}^{im}t_{ml}^{ed*}\delta_a^c + \tfrac{1}{2}P_{(k/l)}\overline{g}_{la}^{mn}t_{mn}^{cd*}\delta_k^i + \tfrac{1}{2}P^{(c/d)}\overline{g}_{ef}^{id}t_{kl}^{ef*}\delta_a^c$$

$$(3.60)$$

$$(I_a^i)_k^l \equiv +f_a^l\delta_k^i - \overline{g}_{ka}^{il} \qquad (I_a^i)_c^d \equiv -f_c^i\delta_a^d + \overline{g}_{ac}^{id} \qquad (3.61)$$

$$(\mathbf{B}_{12})_{ia,klcd} = P^{(k/l)}(I_a^i)_m^k t_{cd}^{ml} - P_{(c/d)}(I_a^i)_c^e t_{ed}^{kl} + P_{(c/d)}^{(k/l)}\overline{g}_{ad}^{le}t_{ce}^{ki} + P_{(c/d)}^{(k/l)}\overline{g}_{md}^{il}t_{ca}^{km} + \overline{g}_{ma}^{kl}t_{cd}^{im}$$

$$+\overline{g}_{cd}^{ie}t_{ae}^{kl}$$

$$(3.62)$$

3.C.2   Blocks of the Metric Matrix

$$(\mathbf{S}_{11})_{ia,jb} = \text{Equation (3.50) with OLCCD density matrices.} \qquad (3.63)$$

3.C.3   Blocks of the Property Gradient Vector

$$(\mathbf{p}_1)_{ia} = \text{Equation (3.51) with OLCCD density matrices.} \qquad (3.64)$$

$$(\mathbf{p}_2)_{ijab} = P_{(a/b)}v_a^e t_{eb}^{ij} - P^{(i/j)}v_m^i t_{ab}^{mj} \qquad (3.65)$$

Table 3.3: Errors in vertical excitation energies (eV) for triplet states computed using LR-OLCCD, LR-ODC-12, and EOM-CCSD, relative to EOM-CCSDT (aug-cc-pVTZ basis set). All electrons were correlated in all computations. Also shown are mean absolute errors (Δ_{MAE}) and standard deviations (Δ_{SD}) computed for each method.

		ΔEOM-CCSD	ΔLR-OLCCD	ΔLR-ODC-12	EOM-CCSDT
N_2	$^3\Sigma_u^+$	0.11	0.04	-0.02	7.63
	$^3\Pi_g$	0.15	0.06	0.11	8.00
	$^3\Delta_u$	0.17	0.08	0.03	8.82
	$^3\Sigma_u^-$	0.28	0.03	0.01	9.63
	$^3\Pi_u$	0.14	-0.01	0.10	11.18
CO	$^3\Pi$	0.12	0.06	0.08	6.27
	$^3\Sigma^+$	0.05	-0.03	-0.03	8.38
	$^3\Delta$	0.11	-0.07	-0.03	9.21
	$^3\Sigma^-$	0.19	-0.18	-0.06	9.72
HCN	$^3\Sigma^+$	0.05	-0.04	-0.10	6.40
	$^3\Delta$	0.13	-0.02	-0.06	7.40
	$^3\Pi$	0.10	0.08	0.06	8.01
	$^3\Sigma^-$	0.16	-0.10	-0.05	8.15
HNC	$^3\Pi$	0.09	0.00	0.03	6.06
	$^3\Sigma^+$	0.04	-0.09	-0.11	7.20
	$^3\Delta$	0.10	-0.14	-0.11	8.02
	$^3\Sigma^+$	0.22	-0.05	0.04	8.38
	$^3\Sigma^-$	0.15	-0.02	0.11	8.56
H_2C_2	$^3\Sigma_u^+$	0.01	-0.02	-0.08	5.52
	$^3\Delta_u$	0.08	-0.02	-0.05	6.41
	$^3\Sigma_u^-$	0.10	-0.03	-0.05	7.10
H_2CO	$^3A_2$	0.04	-0.02	0.01	3.56
	$^3A_1$	0.02	-0.06	-0.14	6.06
Δ_{MAE}		0.05	0.06	0.11	
Δ_{SD}		0.07	0.07	0.06	

[a] For CO, HCN, HNC, and H_2C_2, the $^3\Sigma^-$ ($^3\Sigma_u^-$) excitation energies were obtained from EOM-CC(2,3), which energies were shifted to reproduce the EOM-CCSDT energy for the $^1\Sigma^-$ ($^1\Sigma_u^-$) state.

Chapter 4

Linear-Response Density Cumulant Theory for Excited States: Better Algorithms, Bigger Systems

Figure 4.1: A schematic illustrating the sequence of reduced representations of $\mathbf{E}$ in the algorithm employed in this study. The colored entries must be explicitly computed, whereas the gray entries are determined by Hermitian symmetry.

$$
\begin{array}{|ccc|}
\hline
\mathbf{E}^{(2)} & & \\
\mathbf{E}^{(1)} & & \\
\mathbf{E}^{(0)} & & \\
\mathbf{U}^{(0)\dagger}\mathbf{E}(\mathbf{U}^{(0)}) & \mathbf{U}^{(0)\dagger}\mathbf{E}(\mathbf{U}^{(1)}) & \mathbf{U}^{(0)\dagger}\mathbf{E}(\mathbf{U}^{(2)}) \\
\mathbf{U}^{(1)\dagger}\mathbf{E}(\mathbf{U}^{(0)}) & \mathbf{U}^{(1)\dagger}\mathbf{E}(\mathbf{U}^{(1)}) & \mathbf{U}^{(1)\dagger}\mathbf{E}(\mathbf{U}^{(2)}) \\
\mathbf{U}^{(2)\dagger}\mathbf{E}(\mathbf{U}^{(0)}) & \mathbf{U}^{(2)\dagger}\mathbf{E}(\mathbf{U}^{(1)}) & \mathbf{U}^{(2)\dagger}\mathbf{E}(\mathbf{U}^{(2)}) \\
\hline
\end{array}
$$
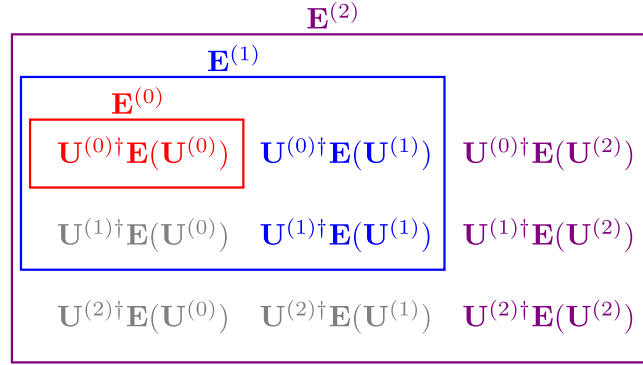
We have implemented the LR-ODC-12 method using a multi-root Davidson algorithm, which solves the linear-response generalized eigenvalue problem by progressively growing an expansion space for the n_{root} lowest generalized eigenvectors of $\mathbf{E}$ and $\mathbf{M}$. The general procedure looks as follows:

1. Initialize the expansion space with a set of $n_{\text{guess}} \geq n_{\text{root}}$ orthonormal vectors.

$$\mathbf{R}^{(0)} = (\mathbf{u}_1^{(0)} \cdots \mathbf{u}_{n_{\text{guess}}}^{(0)})$$

2. Express the energy-Hessian and metric matrices in the reduced expansion space.

$$\mathbf{E}^{(i)} = \mathbf{R}^{(i)\dagger}\mathbf{E}(\mathbf{R}^{(i)})$$

$$\mathbf{M}^{(i)} = \mathbf{R}^{(i)\dagger}\mathbf{M}(\mathbf{R}^{(i)})$$

3. Solve for the n_{root} highest eigenvectors of the inverse eigenvalue equation.

$$\mathbf{M}^{(i)}\mathbf{z}_k^{(i)} = \mathbf{E}^{(i)}\mathbf{z}_k^{(i)}/\omega_k^{(i)}$$

4. Determine the residual for each root.

$$\mathbf{d}_k^{(i)} = \mathbf{M}(\mathbf{z}_k^{(i)}) - \mathbf{E}(\mathbf{z}_k^{(i)})/\omega_k^{(i)}$$

If the residual elements are sufficiently small we consider the eigenvectors converged and exit the loop.

5. Form new direction vectors by preconditioning the residuals.

$$\mathbf{g}_k^{(i+1)} = -(\tilde{\mathbf{M}} - \tilde{\mathbf{E}}/\omega_k^{(i)})^{-1}\mathbf{d}_k$$

The tildes in this equation denote diagonal approximations to these matrices.

64

6. Project out the span of the current expansion space from the new direction vectors.

$$\mathbf{J}^{(i+1)} = (\mathbf{1} - \mathbf{R}^{(i)}\mathbf{R}^{(i)\dagger})(\mathbf{g}_1^{(i+1)} \cdots \mathbf{g}_{n_{\text{root}}}^{(i+1)})$$

7. Determine an orthonormal basis for the new direction vectors using a compressed singular value decomposition, and add these new vectors to the expansion space.

$$\mathbf{J}^{(i+1)} \approx \mathbf{U}^{(i+1)}\boldsymbol{\Sigma}^{(i+1)}\mathbf{V}^{(i+1)\dagger}$$

$$\mathbf{R}^{(i+1)} \leftarrow (\mathbf{R}^{(i)} \ \mathbf{U}^{(i+1)})$$

8. Increment i and return to step 2.

A key feature of this algorithm is that we never need to explicilty construct the energy-Hessian and metric matrices in memory, only their images over the expansion space.

For the diagonal approximations in step 5 we use the following.

$$\tilde{\mathbf{S}}_{11} \equiv \mathbf{1}_1$$

$$(\tilde{\mathbf{A}}_{11})_{ia,ia} \equiv -f_i^i + f_a^a$$

$$(\tilde{\mathbf{A}}_{22})_{ijab,ijab} \equiv -\mathcal{F}_i^i - \mathcal{F}_j^j - \mathcal{F}_a^a - \mathcal{F}_b^b$$

These can also be used to construct the initial expansion space in step 1, namely by including unit vectors for the n_{guess} smallest positive entries in $\tilde{\mathbf{E}}$.

4.0.1 Ethylene, Butadiene, and Hexatriene

Table 4.1: Vertical excitation energies computed using LR-OLCCD, LR-ODC-12, and EOM-CCSD for the low-lying electronic states of ethylene (C_2H_4), butadiene (C_4H_6), and hexatriene (C_6H_8). Computations employed the ANO-L-pVDZ (for C_4H_6 and C_6H_8) and ANO-L-pVTZ (for C_2H_4) basis sets and the MP2/cc-pVQZ optimized geometries. For LR-OLCCD and LR-ODC-12, oscillator strengths of the allowed transitions are given in parentheses. All electrons were correlated in all computations. Also shown are the excitation energies from the frozen-core semistochastic heat-bath CI (SHCI) method, extrapolated to full CI limit.

		EOM-CCSD	LR-OLCCD	LR-ODC-12	SHCI[a]
C_2H_4	$^3B_{1u}$	4.46	4.66	4.52	4.59
	$^1B_{1u}$	8.14	8.20 (1.8)	8.14 (1.9)	8.05
C_4H_6	^3B_u	3.20	3.58	3.43	3.37
	^1B_u	6.53	6.76 (4.2)	6.67 (4.4)	6.45
	^1A_g	7.28	7.14	6.81	6.58
C_6H_8	^3B_u	2.64	3.01	2.83	2.77
	^1B_u	5.60	5.89 (6.5)	5.74 (8.1)	5.59
	^1A_g	6.55		5.73	5.58

[a] The SHCI computations used the same basis sets and optimized geometries as those used for LR-OLCCD, LR-ODC-12, and EOM-CCSD.

Chapter 5

Conclusion

My conclusions.

Bibliography

[1] M. Nooijen, K. R. Shamasundar, and D. Mukherjee, Mol. Phys. **103**, 2277 (2005).

[2] J. A. Pople, J. S. Binkley, and R. Seeger, Int. J. Quantum Chem. **10**, 1 (1976).

[3] R. J. Bartlett, Annu. Rev. Phys. Chem. **32**, 359 (1981).

[4] P. G. Szalay, M. Nooijen, and R. J. Bartlett, J. Chem. Phys. **103**, 281 (1995).

[5] H. P. Kelly and A. M. Sessler, Phys. Rev. **132**, 2091 (1963).

[6] H. P. Kelly, Phys. Rev. A **134**, 1450 (1964).

[7] W. Meyer, J. Chem. Phys. **58**, 1017 (1973).

[8] R. Ahlrichs, Comput. Phys. Commun. **17**, 31 (1979).

[9] S. Koch and W. Kutzelnigg, Theor. Chim. Acta **59**, 387 (1981).

[10] M. Gelus, R. Ahlrichs, V. Staemmler, and W. Kutzelnigg, Chem. Phys. Lett. **7**, 503 (1970).

[11] V. Staemmler and M. Jungen, Chem. Phys. Lett. **16**, 187 (1972).

[12] R. Ahlrichs, F. Driessler, H. Lischka, V. Staemmler, and W. Kutzelnigg, J. Chem. Phys. **62**, 1235 (1975).

[13] H. Kollmar and V. Staemmler, J. Am. Chem. Soc. **99**, 3583 (1977).

[14] J. Wasilewski, V. Staemmler, and S. Koch, Phys. Rev. A **38**, 1289 (1988).

[15] A. G. Taube and R. J. Bartlett, J. Chem. Phys. **130**, 144112 (2009).

[16] F. Coester, Nucl. Phys. **7**, 421 (1958).

[17] F. Coester and H. Kümmel, Nucl. Phys. **17**, 477 (1960).

[18] J. Čížek, J. Chem. Phys. **45**, 4256 (1966).

[19] R. J. Bartlett and G. D. Purvis, Int. J. Quantum Chem. **14**, 561 (1978).

[20] T. D. Crawford and H. F. Schaefer, Rev. Comp. Chem. **14**, 33 (2000).

[21] R. J. Bartlett and M. Musiał, Rev. Mod. Phys. **79**, 291 (2007).

[22] I. Shavitt and R. J. Bartlett, *Many-Body Methods in Chemistry and Physics* (Cambridge University Press, Cambridge, UK, 2009).

[23] C. Kollmar and F. Neese, Mol. Phys. **108**, 2449 (2010).

[24] J. P. Daudey, J. L. Heully, and J. P. Malrieu, J. Chem. Phys. **99**, 1240 (1993).

[25] J. P. Malrieu, H. Zhang, and J. Ma, Chem. Phys. Lett. **493**, 179 (2010).

[26] M. Nooijen and R. J. Le Roy, J. Mol. Struct. **768**, 25 (2006).

[27] C. Kollmar and F. Neese, J. Chem. Phys. **135**, 84102 (2011).

[28] C. Kollmar and A. Heßelmann, Theor. Chem. Acc. **127**, 311 (2010).

[29] U. Bozkaya and C. D. Sherrill, J. Chem. Phys. **139**, 054104 (2013).

[30] E. Soydaŧ and U. Bozkaya, J. Comput. Chem. **35**, 1073 (2014).

[31] U. Bozkaya, J. Chem. Phys. **139**, 154105 (2013).

[32] F. Wennmohs and F. Neese, Chem. Phys. **343**, 217 (2008).

[33] F. Neese, F. Wennmohs, and A. Hansen, J. Chem. Phys. **130**, 114108 (2009).

[34] W. Kutzelnigg, J. Chem. Phys. **125**, 171101 (2006).

[35] D. A. Mazziotti, Phys. Rev. Lett. **101**, 253002 (2008).

[36] D. A. Mazziotti, Phys. Rev. A **81**, 62515 (2010).

[37] A. E. DePrince and D. A. Mazziotti, Mol. Phys. **110**, 1917 (2012).

[38] W. Kutzelnigg and D. Mukherjee, J. Chem. Phys. **107**, 432 (1997).

[39] D. A. Mazziotti, Chem. Phys. Lett. **289**, 419 (1998).

[40] D. A. Mazziotti, Phys. Rev. A **57**, 4219 (1998).

[41] W. Kutzelnigg and D. Mukherjee, J. Chem. Phys. **110**, 2800 (1999).

[42] L. Kong, Int. J. Quantum Chem. **111**, 3541 (2011).

[43] M. Hanauer and A. Köhn, Chem. Phys. **401**, 50 (2012).

[44] M. Nakata and K. Yasuda, Phys. Rev. A **80**, 42109 (2009).

[45] H. van Aggelen, B. Verstichel, P. Bultinck, D. Van Neck, P. W. Ayers, and D. L. Cooper, J. Chem. Phys. **132**, 114112 (2010).

[46] B. Verstichel, H. van Aggelen, D. Van Neck, P. W. Ayers, and P. Bultinck, J. Chem. Phys. **132**, 114113 (2010).

[47] J. M. Herbert and J. E. Harriman, Adv. Chem. Phys. **134**, 261 (2007).

[48] A. C. Simmonett, J. J. Wilke, H. F. Schaefer, and W. Kutzelnigg, J. Chem. Phys. **133**, 174122 (2010).

[49] A. Y. Sokolov, J. J. Wilke, A. C. Simmonett, and H. F. Schaefer, J. Chem. Phys. **137**, 054105 (2012).

[50] W. Kutzelnigg and D. Mukherjee, J. Chem. Phys. **120**, 7350 (2004).

[51] A. Y. Sokolov, A. C. Simmonett, and H. F. Schaefer, J. Chem. Phys. **138**, 024107 (2013).

[52] A. Y. Sokolov and H. F. Schaefer, J. Chem. Phys. **139**, 204110 (2013).

[53] D. A. Mazziotti, ed., *Reduced-Density-Matrix Mechanics: With Application to Many-Electron Atoms and Molecules*, Advances in Chemical Physics, Vol. 134 (John Wiley & Sons, Inc., Hoboken, NJ, 2007).

71

[54] J. M. Turney, A. C. Simmonett, R. M. Parrish, E. G. Hohenstein, F. A. Evangelista, J. T. Fermann, B. J. Mintz, L. A. Burns, J. J. Wilke, M. L. Abrams, N. J. Russ, M. L. Leininger, C. L. Janssen, E. T. Seidl, W. D. Allen, H. F. Schaefer, R. A. King, E. F. Valeev, C. D. Sherrill, and T. D. Crawford, WIREs Comput. Mol. Sci. **2**, 556 (2012).

[55] K. Raghavachari, G. W. Trucks, J. A. Pople, and M. Head-Gordon, Chem. Phys. Lett. **157**, 479 (1989).

[56] J. F. Stanton, Chem. Phys. Lett. **281**, 130 (1997).

[57] T. H. Dunning, J. Chem. Phys. **90**, 1007 (1989).

[58] D. E. Woon and T. H. Dunning, J. Chem. Phys. **103**, 4572 (1995).

[59] R. A. Kendall, T. H. Dunning, and R. J. Harrison, J. Chem. Phys. **96**, 6796 (1992).

[60] J. ÅŸezáč and P. Hobza, J. Chem. Theory Comput. **9**, 2151 (2013).

[61] Y. Zhao, B. J. Lynch, and D. G. Truhlar, Phys. Chem. Chem. Phys. **7**, 43 (2005).

[62] E. SoydaÅ§ and U. Bozkaya, J. Chem. Theory Comput. **9**, 1452 (2013).

[63] B. J. Lynch, Y. Zhao, and D. G. Truhlar, "enquote "bibinfo title The Minnesota Databases for Chemistry and Solid-State Physics," .

[64] H. Zipse, Top. Curr. Chem. **263**, 163 (2006).

[65] E. F. C. Byrd, C. D. Sherrill, and M. Head-Gordon, J. Phys. Chem. A **105**, 9736 (2001).

[66] G. J. O. Beran, S. R. Gwaltney, and M. Head-Gordon, Phys. Chem. Chem. Phys. **5**, 2488 (2003).

[67] R. C. Lochan and M. Head-Gordon, J. Chem. Phys. **126**, 164101 (2007).

[68] W. Kurlancheek and M. Head-Gordon, Mol. Phys. **107**, 1223 (2009).

[69] U. Bozkaya, J. Chem. Phys. **135**, 224103 (2011).

[70] S. G. Lias, J. E. Bartmess, J. F. Liebman, J. L. Holmes, R. D. Levin, and W. G. Mallard, J. Phys. Chem. Ref. Data **17**, 1 (1988).

[71] T. Trickl, E. F. Cromwell, Y. T. Lee, and A. H. Kung, J. Chem. Phys. **91**, 6006 (1989).

[72] Z. Zhang, S. C. Kuo, R. B. Klemm, P. S. Monks, and L. J. Stief, Chem. Phys. Lett. **229**, 377 (1994).

[73] A. Hansel, C. Scheiring, M. Glantschnig, W. Lindinger, and E. E. Ferguson, J. Chem. Phys. **109**, 1748 (1998).

[74] U. Bozkaya and H. F. Schaefer, J. Chem. Phys. **136**, 204114 (2012).

[75] W. Kutzelnigg and D. Mukherjee, J. Chem. Phys. **116**, 4787 (2002).

[76] W. Kutzelnigg, K. R. Shamasundar, and D. Mukherjee, Mol. Phys. **108**, 433 (2010).

[77] H.-J. Werner, F. R. Manby, and P. J. Knowles, J. Chem. Phys. **118**, 8149 (2003).

[78] A. G. Taube and R. J. Bartlett, Collect. Czech. Chem. Commun. **70**, 837 (2005).

[79] F. Neese, A. Hansen, and D. G. Liakos, J. Chem. Phys. **131**, 64103 (2009).

[80] O. Vahtras, J. Almlöf, and M. W. Feyereisen, Chem. Phys. Lett. **213**, 514 (1993).

[81] G. Hetzer, M. Schütz, H. Stoll, and H.-J. Werner, J. Chem. Phys. **113**, 9443 (2000).

[82] M. Schütz and H.-J. Werner, J. Chem. Phys. **114**, 661 (2001).

[83] T. B. Pedersen, H. Koch, and C. Hättig, J. Chem. Phys. **110**, 8318 (1999).

[84] T. B. Pedersen, B. Fernández, and H. Koch, J. Chem. Phys. **114**, 6983 (2001).

[85] P. J. Knowles and H.-J. Werner, Chem. Phys. Lett. **115**, 259 (1985).

[86] H.-J. Werner and P. J. Knowles, J. Chem. Phys. **82**, 5053 (1985).

[87] K. Wolinski, H. L. Sellers, and P. Pulay, Chem. Phys. Lett. **140**, 225 (1987).

[88] K. Hirao, Chem. Phys. Lett. **190**, 374 (1992).

[89] J. P. Finley, P. Å. Malmqvist, B. O. Roos, and L. Serrano-Andrés, Chem. Phys. Lett. **288**, 299 (1998).

[90] K. Andersson, P. Å. Malmqvist, B. O. Roos, A. J. Sadlej, and K. Wolinski, J. Phys. Chem. **94**, 5483 (1990).

[91] K. Andersson, P. Å. Malmqvist, and B. O. Roos, J. Chem. Phys. **96**, 1218 (1992).

[92] H.-J. Werner, Mol. Phys. **89**, 645 (1996).

[93] C. Angeli, R. Cimiraglia, S. Evangelisti, T. Leininger, and J.-P. Malrieu, J. Chem. Phys. **114**, 10252 (2001).

[94] C. Angeli, R. Cimiraglia, and J.-P. Malrieu, Chem. Phys. Lett. **350**, 297 (2001).

[95] D. Mukherjee, R. K. Moitra, and A. Mukhopadhyay, Mol. Phys. **33**, 955 (1977).

[96] I. Lindgren, Int. J. Quantum Chem. **14**, 33 (1978).

[97] P. E. M. Siegbahn, J. Chem. Phys. **72**, 1647 (1980).

[98] B. Jeziorski and H. J. Monkhorst, Phys. Rev. A **24**, 1668 (1981).

[99] H.-J. Werner and P. J. Knowles, J. Chem. Phys. **89**, 5803 (1988).

[100] U. S. Mahapatra, B. Datta, and D. Mukherjee, Mol. Phys. **94**, 157 (1998).

[101] U. S. Mahapatra, B. Datta, and D. Mukherjee, J. Chem. Phys. **110**, 6171 (1999).

[102] J. Pittner, J. Chem. Phys. **118**, 10876 (2003).

75

[103] F. A. Evangelista, W. D. Allen, and H. F. Schaefer, J. Chem. Phys. **127**, 24102 (2007).

[104] D. Datta, L. Kong, and M. Nooijen, J. Chem. Phys. **134**, 214116 (2011).

[105] F. A. Evangelista and J. Gauss, J. Chem. Phys. **134**, 114102 (2011).

[106] A. Köhn, M. Hanauer, L. A. Mück, T.-C. Jagau, and J. Gauss, Wiley Interdiscip. Rev.: Comput. Mol. Sci. **3**, 176 (2013).

[107] M. Nooijen, O. Demel, D. Datta, L. Kong, K. R. Shamasundar, V. Lotrich, L. M. Huntington, and F. Neese, J. Chem. Phys. **140**, 81102 (2014).

[108] J. B. Foresman, M. Head-Gordon, J. A. Pople, and M. J. Frisch, J. Phys. Chem. **96**, 135 (1992).

[109] C. D. Sherrill and H. F. Schaefer, Adv. Quant. Chem. **34**, 143 (1999).

[110] J. Geertsen, M. Rittby, and R. J. Bartlett, Chem. Phys. Lett. **164**, 57 (1989).

[111] D. C. Comeau and R. J. Bartlett, Chem. Phys. Lett. **207**, 414 (1993).

[112] J. F. Stanton and R. J. Bartlett, J. Chem. Phys. **98**, 7029 (1993).

[113] A. I. Krylov, Annu. Rev. Phys. Chem. **59**, 433 (2008).

[114] H. Sekino and R. J. Bartlett, Int. J. Quantum Chem. **26**, 255 (1984).

[115] H. Koch, H. J. A. Jensen, P. Jørgensen, and T. Helgaker, J. Chem. Phys. **93**, 3345 (1990).

[116] H. Koch and P. Jørgensen, J. Chem. Phys. **93**, 3333 (1990).

[117] M. Nooijen and R. J. Bartlett, J. Chem. Phys. **106**, 6441 (1997).

[118] M. Nooijen and R. J. Bartlett, J. Chem. Phys. **107**, 6812 (1997).

[119] H. Nakatsuji and K. Hirao, J. Chem. Phys. **68**, 2053 (1978).

[120] H. Nakatsuji, Chem. Phys. Lett. **67**, 329 (1979).

[121] J. F. Stanton, J. Chem. Phys. **99**, 8840 (1993).

[122] J. F. Stanton and J. Gauss, J. Chem. Phys. **100**, 4695 (1994).

[123] J. F. Stanton and J. Gauss, J. Chem. Phys. **101**, 8938 (1994).

[124] S. V. Levchenko, T. Wang, and A. I. Krylov, J. Chem. Phys. **122**, 224106 (2005).

[125] J. Schirmer, Phys. Rev. A **26**, 2395 (1982).

[126] J. Schirmer, Phys. Rev. A **43**, 4647 (1991).

[127] J. Schirmer and A. B. Trofimov, J. Chem. Phys. **120**, 11449 (2004).

[128] P. H. P. Harbach, M. Wormit, and A. Dreuw, J. Chem. Phys. **141**, 64113 (2014).

[129] A. Dreuw and M. Wormit, WIREs Comput. Mol. Sci. **5**, 82 (2014).

[130] A. G. Taube and R. J. Bartlett, Int. J. Quantum Chem. **106**, 3393 (2006).

[131] D. Kats, D. Usvyat, and M. Schütz, Phys. Rev. A **83**, 62503 (2011).

[132] G. Wälz, D. Kats, D. Usvyat, T. Korona, and M. Schütz, Phys. Rev. A **86**, 52519 (2012).

[133] E. F. Kjønstad and H. Koch, J. Phys. Chem. Lett. **8**, 4801 (2017).

[134] R. Moszynski, P. S. Żuchowski, and B. Jeziorski, Collect. Czech. Chem. Commun. **70**, 1109 (2005).

[135] T. Korona, Phys. Chem. Chem. Phys. **12**, 14977 (2010).

[136] A. Y. Sokolov, H. F. Schaefer, and W. Kutzelnigg, J. Chem. Phys. **141**, 74111 (2014).

[137] X. Wang, A. Y. Sokolov, J. M. Turney, and H. F. Schaefer, J. Chem. Theory Comput. **12**, 4833 (2016).

[138] P. Fulde, *Electron Correlations in Molecules and Solids* (Springer, Berlin, 1991).

[139] P. Ziesche, Solid State Commun **82**, 597 (1992).

[140] P. Ziesche, in *Many-Electron Densities and Reduced Density Matrices*, edited by J. Cioslowski (Springer US, Boston, MA, 2000) pp. 33–56.

[141] L. Kong and E. F. Valeev, J. Chem. Phys. **134**, 214109 (2011).

[142] F. Colmenero and C. Valdemoro, Phys. Rev. A **47**, 979 (1993).

[143] H. Nakatsuji and K. Yasuda, Phys. Rev. Lett. **76**, 1039 (1996).

[144] D. A. Mazziotti, Phys. Rev. Lett. **97**, 143002 (2006).

[145] C. Kollmar, J. Chem. Phys. **125**, 84108 (2006).

[146] A. E. DePrince and D. A. Mazziotti, Phys. Rev. A **76**, 42501 (2007).

[147] A. E. DePrince, J. Chem. Phys. **145**, 164109 (2016).

[148] W. Kutzelnigg, Theor. Chim. Acta **80**, 349 (1991).

[149] W. Kutzelnigg, Mol. Phys. **94**, 65 (1998).

[150] T. Van Voorhis and M. Head-Gordon, J. Chem. Phys. **113**, 8873 (2000).

[151] W. Kutzelnigg, J. Chem. Phys. **77**, 3081 (1982).

[152] R. J. Bartlett, S. A. Kucharski, and J. Noga, Chem. Phys. Lett. **155**, 133 (1989).

[153] J. D. Watts, G. W. Trucks, and R. J. Bartlett, Chem. Phys. Lett. **157**, 359 (1989).

[154] B. Cooper and P. J. Knowles, J. Chem. Phys. **133**, 234102 (2010).

[155] F. A. Evangelista, J. Chem. Phys. **134**, 224102 (2011).

[156] A. C. Scheiner, G. E. Scuseria, J. E. Rice, T. J. Lee, and H. F. Schaefer, J. Chem. Phys. **87**, 5361 (1987).

[157] E. A. Salter, G. W. Trucks, and R. J. Bartlett, J. Chem. Phys. **90**, 1752 (1989).

[158] J. Gauss, J. F. Stanton, and R. J. Bartlett, J. Chem. Phys. **95**, 2623 (1991).

[159] J. Gauss, W. J. Lauderdale, J. F. Stanton, J. D. Watts, and R. J. Bartlett, Chem. Phys. Lett. **182**, 207 (1991).

[160] A. V. Copan, A. Y. Sokolov, and H. F. Schaefer, J. Chem. Theory Comput. **10**, 2389 (2014).

[161] J. W. Mullinax, A. Y. Sokolov, and H. F. Schaefer, J. Chem. Theory Comput. **11**, 2487 (2015).

[162] P. Norman, Phys. Chem. Chem. Phys. **13**, 20519 (2011).

[163] T. Helgaker, S. Coriani, P. Jørgensen, K. Kristensen, J. Olsen, and K. Ruud, Chem. Rev. **112**, 543 (2012).

[164] K. Kristensen, J. Kauczor, T. Kjærgaard, and P. Jørgensen, J. Chem. Phys. **131**, 044112 (2009).

[165] J. Olsen and P. Jørgensen, J. Chem. Phys. **82**, 3235 (1985).

[166] S. P. A. Sauer, *Molecular Electromagnetism: A Computational Chemistry Approach* (Oxford University Press, Oxford, 2011).

[167] R. M. Parrish, L. A. Burns, D. G. A. Smith, A. C. Simmonett, A. E. DePrince, E. G. Hohenstein, U. Bozkaya, A. Y. Sokolov, R. Di Remigio, R. M. Richard, J. F. Gonthier, A. M. James, H. R. McAlexander, A. Kumar, M. Saitow, X. Wang, B. P. Pritchard, P. Verma, H. F. Schaefer, K. Patkowski, R. A. King, E. F. Valeev, F. A. Evangelista, J. M. Turney,

T. D. Crawford, and C. D. Sherrill, J. Chem. Theory Comput. **13**, 3185 (2017).

[168] Q. Sun, T. C. Berkelbach, N. S. Blunt, G. H. Booth, S. Guo, Z. Li, J. Liu, J. D. McClain, E. R. Sayfutyarova, S. Sharma, S. Wouters, and G. K.-L. Chan, WIREs Comput. Mol. Sci. **8**, e1340 (2018).

[169] E. R. Davidson, J. Comput. Phys. **17**, 87 (1975).

[170] B. Liu, "The Simultaneous Expansion Method for the Iterative Solution of Several of the Lowest-Lying Eigenvalues and Corresponding Eigenvectors of Large Real-Symmetric Matrices," Tech. Rep. (Lawrence Berkeley Laboratory, University of California, Berkeley, CA, USA, 1978).

[171] Y. Shao, Z. Gan, E. Epifanovsky, A. T. Gilbert, M. Wormit, J. Kussmann, A. W. Lange, A. Behn, J. Deng, X. Feng, D. Ghosh, M. Goldey, P. R. Horn, L. D. Jacobson, I. Kaliman, R. Z. Khaliullin, T. KuÅŻ, A. Landau, J. Liu, E. I. Proynov, Y. M. Rhee, R. M. Richard, M. A. Rohrdanz, R. P. Steele, E. J. Sundstrom, H. L. W. III, P. M. Zimmerman, D. Zuev, B. Albrecht, E. Alguire, B. Austin, G. J. O. Beran, Y. A. Bernard, E. Berquist, K. Brandhorst, K. B. Bravaya, S. T. Brown, D. Casanova, C.-M. Chang, Y. Chen, S. H. Chien, K. D. Closser, D. L. Crittenden, M. Diedenhofen, R. A. D. Jr., H. Do, A. D. Dutoi, R. G. Edgar, S. Fatehi, L. Fusti-Molnar, A. Ghysels, A. Golubeva-Zadorozhnaya, J. Gomes, M. W. Hanson-Heine, P. H. Harbach, A. W. Hauser, E. G. Hohenstein, Z. C. Holden, T.-C. Jagau, H. Ji, B. Kaduk, K. Khistyaev, J. Kim, J. Kim, R. A. King, P. Klunzinger, D. Kosenkov,

T. Kowalczyk, C. M. Krauter, K. U. Lao, A. D. Laurent, K. V. Lawler, S. V. Levchenko, C. Y. Lin, F. Liu, E. Livshits, R. C. Lochan, A. Luenser, P. Manohar, S. F. Manzer, S.-P. Mao, N. Mardirossian, A. V. Marenich, S. A. Maurer, N. J. Mayhall, E. Neuscamman, C. M. Oana, R. Olivares-Amaya, D. P. OâĂŹNeill, J. A. Parkhill, T. M. Perrine, R. Peverati, A. Prociuk, D. R. Rehn, E. Rosta, N. J. Russ, S. M. Sharada, S. Sharma, D. W. Small, A. Sodt, T. Stein, D. StÃijck, Y.-C. Su, A. J. Thom, T. Tsuchimochi, V. Vanovschi, L. Vogt, O. Vydrov, T. Wang, M. A. Watson, J. Wenzel, A. White, C. F. Williams, J. Yang, S. Yeganeh, S. R. Yost, Z.-Q. You, I. Y. Zhang, X. Zhang, Y. Zhao, B. R. Brooks, G. K. Chan, D. M. Chipman, C. J. Cramer, W. A. G. III, M. S. Gordon, W. J. Hehre, A. Klamt, H. F. S. III, M. W. Schmidt, C. D. Sherrill, D. G. Truhlar, A. Warshel, X. Xu, A. Aspuru-Guzik, R. Baer, A. T. Bell, N. A. Besley, J.-D. Chai, A. Dreuw, B. D. Dunietz, T. R. Furlani, S. R. Gwaltney, C.-P. Hsu, Y. Jung, J. Kong, D. S. Lambrecht, W. Liang, C. Ochsenfeld, V. A. Rassolov, L. V. Slipchenko, J. E. Subotnik, T. V. Voorhis, J. M. Herbert, A. I. Krylov, P. M. Gill, and M. Head-Gordon, Mol. Phys. **113**, 184 (2015).

[172] M. Kállay, Z. Rolik, J. Csontos, P. Nagy, G. Samu, D. Mester, J. Csóka, B. Szabó, I. LadjÃąnszki, L. Szegedy, B. Ladóczki, K. Petrov, M. Farkas, P. D. Mezei, and B. HÃĺgely., "Mrcc, a quantum chemical program suite." See also: Z. Rolik, L. Szegedy, I. Ladjánszki, B. Ladóczki, and M. Kállay, J. Chem. Phys. 139, 094105 (2013), as well as: www.mrcc.hu.

[173] P.-O. Widmark, P. Å. Malmqvist, and B. O. O. Roos, Theoret. Chim. Acta

77, 291 (1990).

[174] C. Daday, S. Smart, G. H. Booth, A. Alavi, and C. Filippi, J. Chem. Theory Comput. **8**, 4441 (2012).

[175] P. M. Zimmerman, J. Phys. Chem. A **121**, 4712 (2017).